Available online at www.sciencedirect.com
SCIENCE DIRECT®
Journal of Chromatography A, 1037 (2004) 125–145
JOURNAL OF CHROMATOGRAPHY A
www.elsevier.com/locate/chroma

Review

Determination of chemical kinetic properties of heterogeneous catalysts

Nicholas A. Katsanos*

Department of Chemistry, University of Patras, P.O. Box 1045, GR-265 04 Patras, Greece

Abstract

The importance of cooperation of heterogeneous catalysis with surface science is stressed for simultaneous adsorptive and catalytic measurements. Inverse gas chromatography and reversed-flow gas chromatography offer a suitable research ground for such collaboration. After a short introduction, adsorption physicochemical quantities of heterogeneous catalysts with typical recent results, chemical kinetic properties and surface energy of catalysts are described, stressing the important aspect of time-resolved chromatography, due to the heterogeneity of the solid surface of catalysts. Adsorption energies, local monolayer capacities, local isotherms and energy distribution functions are extensively described. Also, lateral molecular interactions, surface diffusion and adsorption rates on heterogeneous catalysts are described.

Keywords: Reviews; Kinetic studies; Catalysts; Time-resolved chromatography; Inverse gas chromatography; Reversed-flow gas chromatography; Lateral interactions; Surface diffusion; Adsorption rates; Surface energy

Contents

1. Introduction

Heterogeneous catalysis and surface science are integrally linked and often difficult to distinguish, in spite of the fact that these two fields have evolved from quite opposite perspectives. Surface science has been developed from the study of gas–solid interaction at well-characterized single-crystal surfaces, but the knowledge gained from these simple model systems has made it clear that surface science must move to study reactions on more complex surfaces under more realistic conditions. On the other hand, catalysis that deals with complex reactions on supported metals has been increasingly concerned with identifying fundamental steps that control reaction kinetics and selectivities. These elementary reaction steps call surface science to move to study reactions on more complex surfaces under more realistic conditions. Gas chromatography is a promising "meeting place" of the two above disciplines, one of which is an important part of the technology that supports industrially developed societies. It is, however, disappointing that in a relatively recent (1992) booklet on surface science of catalysis [1], developed from a symposium of American Chemical Society, not a single mention of a gas chromatographic technique is made in the

* Tel.: +30-2610-997110; fax: +30-2610-997144.
E-mail address: katsanos@otenet.gr (N.A. Katsanos).

0021-9673/$ – see front matter © 2004 Elsevier B.V. All rights reserved.
doi:10.1016/j.chroma.2003.11.051

22 papers presented, apart from possible analytic experiments. In contrast to that, a review of 1998 [2] presents some promising examples of collaboration between heterogeneous catalysis and gas chromatography, not only from the point of view of determination of catalytic rate constants, but also for simultaneous diffusion, adsorption and catalytic applications. Such inverse gas chromatography (IGC), used to derive only properties of the stationary phase, has been recently (2001) the object of a 1st International Conference, but from the relevant proceedings [3] one sees that limited work on heterogeneous catalysis by IGC has been presented.

One point, however, is worth mentioning. Time-resolved chemistry on heterogeneous solid surfaces by IGC has entered on the stage [4]. The first relevant publication [5] showed that this was created by trying to overcome the difficulty or rather impossibility of obtaining by any other means an analytical solution of the classical integral equation

$$\Theta(p, T) = \int_0^\infty \theta_i(p, T, \varepsilon)\, f(\varepsilon)\, \mathrm{d}\varepsilon \tag{1}$$

where $\Theta(p, T)$ is the overall adsorption isotherm, unless approximations are used for the local adsorption isotherm $\theta_i(p, T, \varepsilon)$, and/or the adsorption energy distribution function $f(\varepsilon)$. This problem has been somehow extensively described in paragraph 5.4 of the review mentioned [2].

Before going into a detailed description of time-resolved chromatography, it is constructing to summarize some recent achievements of IGC, in spite of the advantages and limitations of the gas chromatographic reactors, as summarized by Conder and Young a long time ago [6]. They refer to adsorption isotherms [7–9], and surface energy [10–13]. It is rather amazing that physicochemical properties so closely connected to heterogeneous catalysis have not been used for gas chromatographic studies of kinetic catalytic properties, as can be judged from the recent symposium on IGC [3]. Following Aristotle that one cannot find the truth without the relevant reason, the present article will try to answer the above question too.

Several papers, books and Symposia had as main objective the heterogeneity of the solid surfaces, like that of Rudzinski and Everett [14]. When, however, describe gas chromatographic techniques, almost all stop to adsorption properties and do not go into catalytic properties. Why is that? An answer obvious to the present author is that gas chromatography, being a continuous dynamic process, presents facts not showing up in classical traditional experiments with solid catalysts and these facts are difficult to be explained. Where do they come from and how can be explained? A possible answer is that IGC provides physicochemical properties of the stationary phase statistically weighed over time and showing up under the chromatographic elution peaks. Some of these properties are indeed independent of time, but there are other properties strongly dependent on the time variable. These are mostly attributed to the heterogeneity of the solid surfaces, but all efforts to measure such quantities with traditional gas chromatography were based on rather crude

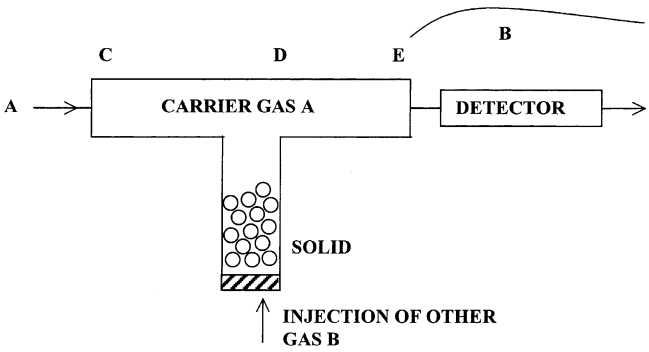

Fig. 1. A schematic representation of the reversed-flow gas chromatography arrangement. (A) denotes the carrier gas, while (B) is another gas (injected or recorded); (C), (D) and (E) are three points of the chromatographic column.

approximations. Thus, one either abandons time-resolved phenomena due to surface heterogeneity or abandons chromatography, as a mean to measure them. Not necessarily thow, since one may remove the main chromatographic term $-u\partial c_\mathrm{m}/\partial x$ from the gas chromatographic equation (u being the carrier gas flow rate, c_m the gaseous analyte concentration, and x the column length co-ordinate), so that the carrier gas flow does not intervene with the measurement of the desired physicochemical quantities. This is the reversed-flow version of gas chromatography (RF-GC) which has already been reviewed in 1998 [2], 2000 [15] and 2002 [4]. This method does not abolish the carrier gas flow, otherwise it would not be “chromatography”, but it places its running direction perpendicularly and a little far from the solid bed, in which all the desired physicochemical phenomena take place (Fig. 1). Thus, the gas–solid boundary surface is confined in a region where no gas is running. This only diffuses slowly from the region of the solid to the horizontal tube through which the carrier gas is normally running. There is, however, an important difference between the carrier gas diffusing out of the vertical column and the “same” gas running through the horizontal tube towards the detector. The latter is a pure carrier gas, whereas the first contains other gases or vapors, like the injected B or those produced on the gas–solid interface. It is to those other gases that the method turns its observation and measurement.

What then one sees in the detector signal? After a short time interval from the injection of B, a broad extented and usually asymmetrical band of B and/or other gases are recorded, as shown in Fig. 1. What is hidden under this broadband, substances or phenomena? Both, but it is difficult to separate them. They refer to the solid surface and the injected substance B, and are carried to the detector by the carrier gas A as this passes by the junction of the horizontal and the vertical tube. If, however, one reverses the direction of the carrier gas flow for a short time period (5–60 s), so short that the gas molecules at the point D cannot manage to reach point C and go out, and then the normal direction of the gas flow is restored again, what would one see in the detector signal? Something like the chromatogram shown

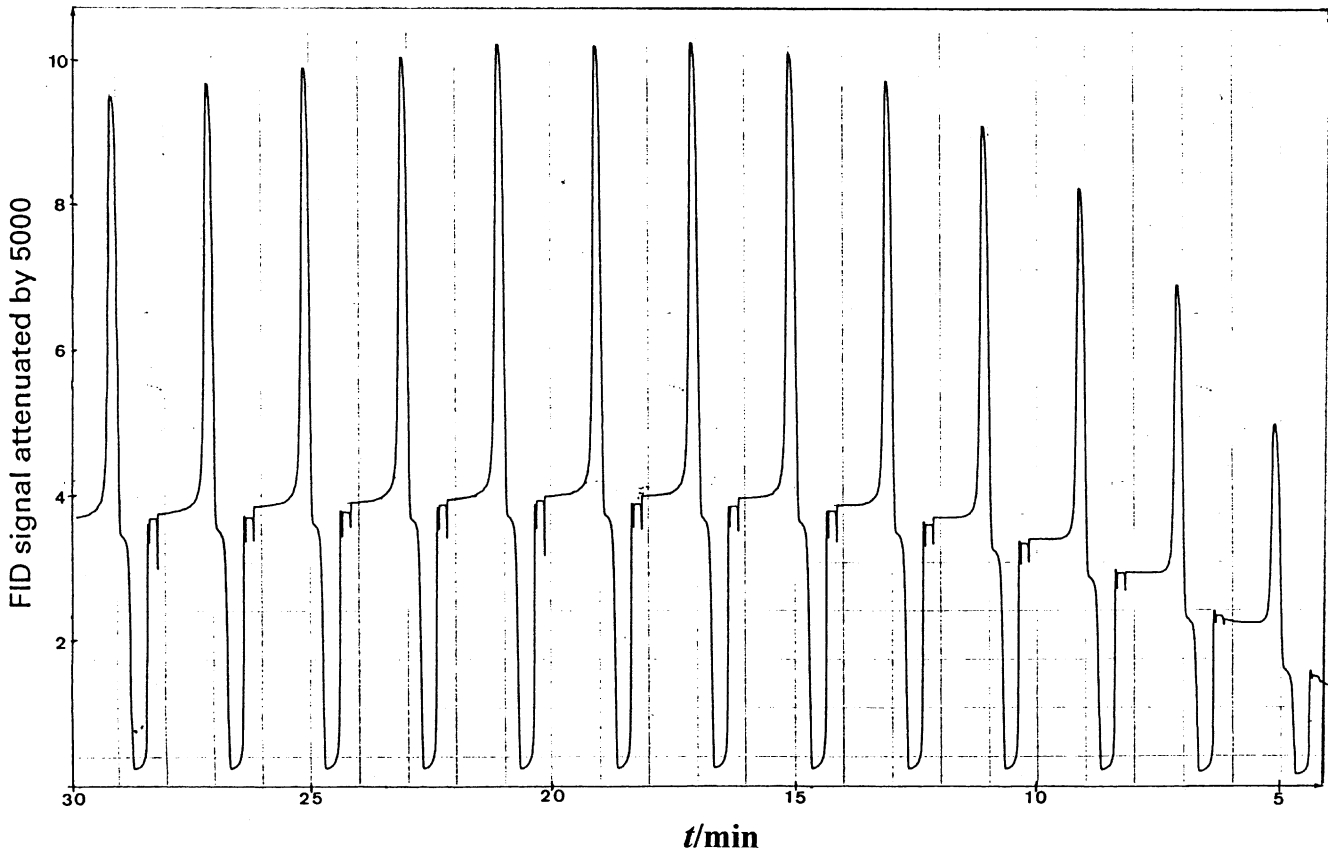

Fig. 2. Sample peaks of propene in nitrogen carrier gas, with vertical tube containing 0.67 g TiO_2, at 323.2 K, and a flame ionization detector.

in Fig. 6 of [2], where B was propene and a flow reversal for 15 s was made to the carrier gas nitrogen running with a $\dot{V}_c = 22\,cm^3/min$. The extra "sample peaks" are due to the flow reversals and have a width at half-height exactly equal to the flow reversal, i.e., 15 s. If the reversal is repeated, many sample peaks appear and so on, as Fig. 2 shows.

They have different heights depending on the time at which each flow reversal was made. The experimental details by means of which the reversals are effected are shown in Fig. 3. They are based on the use of a four-port gas sampling valve connected to the T shape cell as shown. An extra separation chromatographic column may be used, if one wants to separate the components, if any, of each extra sample peak. But first let us explain the formation of the extra peaks, like those in Fig. 2, which by the way are real experimental recording and not theoretical assumptions. Qualitatively, it is easy to say that, as the gaseous contents in the vertical column slowly diffuse into the sampling column (cf. Fig. 3), a certain amount of it is taken off by the flow reversal of the carrier gas as it runs from $x = l' + l$ towards $x = 0$

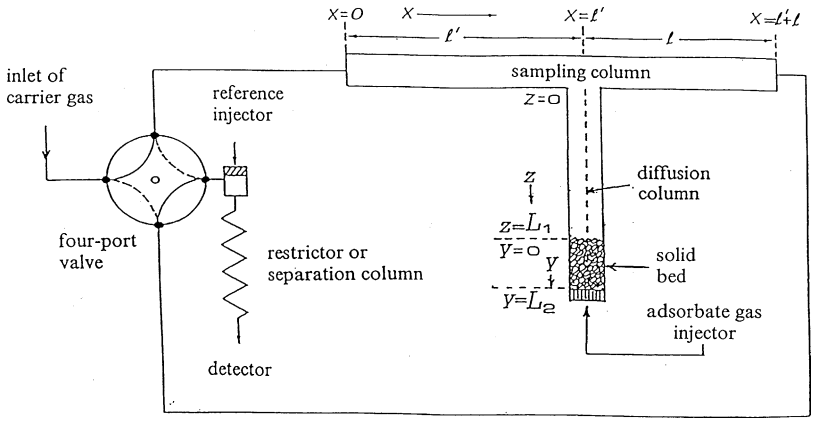

Fig. 3. Schematic representation of the columns and gas connections showing the principle for using the reversed-flow technique as an inverse gas chromatographic tool.

and then from $x = 0$ back towards $x = l' + l$ when its flow is restored to the original direction. It is the amount during this "journey" which is recorded under each extra sample peak of Fig. 2. This has been predicted mathematically by Eqs. (3-19) of [16], solving an ordinary differential equation with Laplace transformations. The solution predicts extra squared peaks when reversing the flow, while the peaks actually obtained are not square owing most probably to non ideality, e.g., axial diffusion in the horizontal section.

The extra peaks obtained by repeatedly reversing the carrier gas direction for short time intervals are termed *sample peaks*, because they constitute samples of the phenomena taken from the region of their occurrence at various times, like small samples taken from a reaction occurring in a usual chemical flask containing the reactants. Since this happens at various chosen times, it constitutes a time-resolved experiment like those in chemical kinetics.

From the series of the sample peaks obtained under various conditions, several physicochemical quantities have been determined and published [2,4,5,8,15,16].

The experimental arrangement sometimes differed a little from that of Fig. 3. In all cases, however, the equation describing the height of the sample peaks H as a function of time t when the flow-reversal was made has the form:

$$H^{1/M} = \sum_i A_i \exp(B_i t) \tag{2}$$

where i runs from 1 to 3 or 4, M is the known response factor of the detector used ($M = 1$ for a flame ionization detector), and A_i, B_i are functions of the physicochemical quantities pertaining to the various phenomena occurring in the solid bed region. The detailed content of A_i and B_i, as found from a non-linear least-square analysis of the plot of $H^{1/M}$ versus time t, leads to the clear determination of the physicochemical quantities of the mathematical model used, e.g., catalytic reaction rate constants, adsorption–desorption rate constants, gas and surface diffusion coefficients, adsorption isotherm parameters, et al., as will be explained analytically in the next sections.

Examples of other experimental methods for determining kinetic catalytic properties by elution gas chromatography have been collected in Table 3 of Review [2]. Here, we shall stress the recent new aspect of RF-GC, i.e., the time-resolved chromatography related to kinetic properties of heterogeneous catalysts.

2. Adsorption physicochemical quantities of heterogeneous catalysts

2.1. Historical review of $f(\varepsilon)$ calculations

The main source of physicochemical information obtained experimentally by gas chromatography (GC) is the broadening of the chromatographic elution peaks, and the analysis of their statistical moments. However, classical GC systems are not in true equilibrium during the retention period, needing extrapolation to infinite dilution and zero carrier gas flow rate to approximate true equilibrium parameters. An acceptable precision of the quantities determined is a difficult, if not impossible, task in many cases.

During the last decade, inverse gas–solid chromatography (IGC) was employed for characterizing heterogeneous solids by calculating adsorption energy distribution functions from retention volume data, the subject being recently reviewed [2]. One is impressed by the various ways used to overcome the difficulty or rather impossibility of obtaining an analytical solution of the classical integral Eq. (1). The difficulties faced led scientists to turn into numerical solutions and estimations [17–22] of $f(\varepsilon)$, which open another way to the problem solution, but these need powerful computers not easily available everywhere.

Very few equations in physical chemistry have remained without a clear proper solution for so long as Eq. (1), i.e., a clear way for calculating $f(\varepsilon)$ from the only experimental quantity $\Theta(p, T)$. Eq. (1) connects the functions $\Theta(p, T)$, $\theta(p, T, \varepsilon)$, and $f(\varepsilon)$ and in principle, if any *two* are known or can be assumed, the remaining one can be calculated. Many choices of such pairs of functions have been examined and designed so that a solution can be found, as described in detail in two books [14,23].

As summarized in a recent publication of us [24], for the local isotherm $\theta(p, T, \varepsilon)$, the simplest and oldest form chosen is the condensation approximation (CA) which assumes a *condensation isotherm*, which is simply a step function with the value 0 for $p < p_c$, and 1 for $p > p_c$, p_c being known as the condensation pressure. The second frequent choice for $\theta(p, T, \varepsilon)$ is the Langmuir isotherm, which lends itself to the use of an integral mathematical transform (the Stieltjes transform) to solve Eq. (1). As regards the distribution function $f(\varepsilon)$, rectangular forms, simple exponentials, Gaussian types, etc. have been tried. It must be repeated, however, that the only experimental information for the systems studied comes from the experimental isotherms $\Theta(p, T)$ at a wide range of pressures, covering four of five orders of magnitude. As Adamson puts it in the recent edition of his book [25], "The field has become somewhat of a happy hunting ground for physical chemists. . . ", or in a recent wonderful review on the subject [26], "The flavor of submonolayer adsorption studies is one of physical chemistry at its best; . . . It is a fine era". The same author, however, [26] adds "it is misleading to talk about a true $f(\varepsilon)$, and any pair of $f(\varepsilon)$ and $\theta(p, T, \varepsilon)$ functions that reproduces $\Theta(p, T)$ within about the experimental error must be acceptable".

In the numerical methods of evaluating the adsorption energy distribution, as covered at length by Chapter 11 of [14], the method of Adamson and Ling [27] forms the starting point for many of the most widely used methods of evaluating the adsorption energy distribution from experimental adsorption isotherms. It was based on a series of successive approximations performed graphically. Later House and Jaycock [28] modified this method, developing a computer

program named HILDA. A recent numerical solution is that of Jagiello [29].

Coming now to the use of IGC for calculating $f(\varepsilon)$, this is based either on a combination of the net retention volume V_N with the crude CA (condensation approximation) or on a more exact solution by the so-called ACCA (asymptotically correct condensation approximation) method. This is based on replacing the true kernel $\theta(p, T, \varepsilon)$ of the integral Eq. (1) by the combination of a Henry and a step isotherm:

$$\theta_{\mathrm{ACCA}} = \begin{cases} \left(\frac{p}{K}\right) \exp\left(\frac{\varepsilon}{kT}\right), & \varepsilon < \varepsilon_c(p, T) \\ 1, & \varepsilon \geq \varepsilon_c(p, T) \end{cases} \tag{3}$$

In terms of V_N, the final solution takes the form

$$f_{\mathrm{ACCA}}(\varepsilon) = -\left(\frac{j}{N_m}\right)\left(\frac{p}{kT}\right)^2\left(\frac{\partial V_N}{\partial p}\right) \tag{4}$$

where j is the James–Martin compressibility factor and N_m the monolayer capacity of the surface. Some other improvements of $f_{\mathrm{ACCA}}(\varepsilon)$ have been reported [14].

From all the above and other literature, one may easily come to the conclusion that so far almost all trials to find $f(\varepsilon)$ are based on the integral Eq. (1). This is not true, however, since in some recent papers of ours [5,30–32] we have employed the inverse gas chromatographic tool RF-GC. The recent review [15] on that is worth mentioning. All determinations by us concerning adsorption onto heterogeneous surfaces [5,30–32] are based on experimental chromatographic data, under one single assumption, namely, that the local isotherm $\theta(p, T, \varepsilon)$ obeys the Javanovic isotherm model [33]. It is well known that this goes over to the Langmuir isotherm in middle pressures and to a linear form at low pressures. The whole treatment of experimental data is based on the fact that these are described by a clear function of time comprising the sum of three or four simple exponentials (Eq. (2)).

2.2. Physicochemical quantities concerning catalysts by the RF-GC method

It is better to start by a solution of the basic Eq. (2) which forms the bridge between experimental chromatographic quantities and physicochemical quantities pertaining to heterogeneous catalysts. In the previous review [2], the solutions described were based on both, a four term solution comprising the sum of four exponential functions, and another solution with three exponential functions [$i = 1$–3 in Eq. (2)]. However, the latter solution, although it has a better repeatability, it was based on a steady-state approximation $\partial c_s/\partial t = 0$ for the adsorbed concentration c_s (mol/g) of the adsorbate [34]. In some applications such a constancy in c_s cannot be assumed, e.g., when measuring surface diffusion coefficients [35]. In such cases, another route was sought, which leads to three exponential functions ($i = 1$–3) in Eq. (2), without employing the steady-state $\partial c_s/\partial t = 0$. The same solution has been also employed in measuring adsorption rates with lateral interaction [36], the time distribution of surface energy [37], and the surface energy of solid catalysts [38]. This solution can also be used for measuring catalytic characteristics, and for this reason a summary of it is given below.

The system of the relevant partial differential equations is:

$$\frac{\partial c_z}{\partial t} = D_z \frac{\partial^2 c_z}{\partial z^2} \tag{5}$$

where c_z is the concentration of the gaseous adsorbate A as function of time t and coordinate z along the diffusion column L_1 (cf. Fig. 3) and D_z denoting the diffusion coefficient of A in this column;

$$\frac{\partial c_y}{\partial t} = D_y \frac{\partial^2 c_y}{\partial y^2} + k_R \frac{a_s}{a_y}(c_s - c_s^*) \tag{6}$$

where c_y is the gaseous concentration of A in the solid bed section L_2 as function of time t and co-ordinate y along the solid bed, D_y the effective diffusion coefficient in section L_2, k_R the adsorption–desorption rate constant on the solid adsorbent, a_s the amount of solid per unit length of bed L_2, a_y the cross-sectional area in the solid bed, c_s the adsorbed concentration of A, and c_s^* the absorbed equilibrium concentration on the solid surface;

$$\frac{\partial c_s}{\partial t} = k_R(c_s^* - c_s) - k_2 c_s \tag{7}$$

describes the rate of change of the adsorbed A, k_2 being the first-order or pseudo-first-order rate constant of a possible surface reaction; finally, the above system includes the isotherm of the locally adsorbed c_s^*:

$$c_s^* = \frac{a_y}{a_s} k_1 \int_0^t c_y(\tau)\, \mathrm{d}\tau \tag{8}$$

k_1 being a dynamic adsorption rate constant and τ a dummy variable for time.

The system of Eqs. (5)–(8) can be solved by taking double Laplace transforms of the four equations with respect to t (parameter p) and with respect to z or y (parameter s).

With the help of the initial and boundary conditions valid for the experimental arrangement and the conducting of the measurements, the above system of equations leads to the following expression for the Laplace transform with respect to time of the gaseous concentration $C(l', p)$ of the adsorbate as recorded by the chromatographic detector. For the details of the derivation, one may consult [35,37]:

$$C(l', p) = \frac{G(p^2 + kp)}{p^3 + X_1 p^2 + Y_1 p + Z_1} = \frac{G(p^2 + kp)}{(p - B_1)(p - B_2)(p - B_3)} \tag{9}$$

where

$$G = \frac{n_A a_1 a_2}{\dot{V}(a_1 + a_2 + a_2 Q)} \tag{10}$$

$$a_1 = \frac{2D_z}{L_1^2}, \qquad a_2 = \frac{2D_y}{L_2^2}, \qquad Q = \frac{2a_y L_2}{a_z L_1} \tag{11}$$

$$k = k_2 + k_R \tag{12}$$

and B_1, B_2, B_3 are the roots of the third degree polynomial $p^3 + X_1 p^2 + Y_1 p + Z_1$, the X_1, Y_1 and Z_1 parameters being given by the relations:

$$X_1 = \frac{a_1 a_2}{a_1 + a_2 + a_2 Q} + k = -(B_1 + B_2 + B_3) \tag{13}$$

$$Y_1 = \frac{a_1 a_2 k + (a_1 + a_2 Q) k_1 k_R}{a_1 + a_2 + a_2 Q} = B_1 B_2 + B_1 B_3 + B_2 B_3 \tag{14}$$

$$Z_1 = \frac{a_1 + a_2 Q}{a_1 + a_2 + a_2 Q} k_1 k_2 k_R = -B_1 B_2 B_3 \tag{15}$$

The aim of the above manipulations was to obtain a form, the inverse Laplace transformation of which with respect to p is easily found with an acceptable precision. This is the far right form of Eq. (9), the inverse transform of which is found in published tables as:

$$c(l', t) = G \sum_{i=1}^{3} A_i^0 \exp(B_i t) \tag{16}$$

where

$$A_1^0 = \frac{B_1^2 + kB_1}{(B_1 - B_2)(B_1 - B_3)},$$
$$A_2^0 = \frac{B_2^2 + kB_2}{(B_2 - B_1)(B_2 - B_3)},$$
$$A_3^0 = \frac{B_3^2 + kB_3}{(B_3 - B_1)(B_3 - B_2)} \tag{17}$$

Eq. (16) has exactly the right-hand side form of Eq. (2), the sample peak height H taken as analogous to the gaseous recorded concentration $c(l', t)$ with proportionality constant g, G being given by the independent of time Eq. (10) and thus $gGA_i^0 = A_i$ of Eq. (2).

$$H^{1/M} = gG \sum_{i=1}^{3} A_i^0 \exp(B_i t) \tag{18}$$

It follows that the ratio of any two A_i equals to the corresponding ratio of A_i^0.

2.2.1. Calculation of rate constants and diffusion coefficients

By means of a GW-BASIC computer program already published as Appendix A in [39], a non-linear least squares method gives the values of A_1, A_2, A_3 and B_1, B_2, B_3 of Eq. (2) from the experimental measurement of the pairs H, t, entered in the DATA lines. A slightly modified program of this is listed as Appendix A here, having an additional loop to choose the number of listed DATA (lines 3000–3040) corresponding to the highest possible square correlation coefficient.

From the A_i (i = 1–3) values found and printed in lines 1020–1090, first the k value of Eq. (12) is calculated from the next ratios obtained by Eq. (17):

$$\frac{A_2^0 (B_2 - B_1)(B_2 - B_3)}{A_1^0 (B_1 - B_2)(B_1 - B_3)} = \frac{B_2^2 + kB_2}{B_1^2 + kB_1} \tag{19}$$

$$\frac{A_3^0 (B_3 - B_1)(B_3 - B_2)}{A_1^0 (B_1 - B_2)(B_1 - B_3)} = \frac{B_3^2 + kB_3}{B_1^2 + kB_1} \tag{20}$$

Using the mean of the k values obtained from the above two equations, and the a_1 value of Eq. (11) from the literature value of D_z [40] and the known L_1 value, one easily finds a_2 using Eq. (13) and the value of X_1 calculated from $B_1 + B_2 + B_3$.

With the help of Eq. (14), $k_1 k_R$ is calculated, and from Eq. (15) $k_1 k_2 k_R$ is found. Division of the latter two gives k_2, and subtraction of it from k gives k_R according to Eq. (12). Finally, division of $k_1 k_R$ by k_R gives k_1. Thus, k_1, k_2, k_R and D_y (from a_2) are all obtained directly from the values of A_1, A_2, A_3, B_1, B_2, B_3, as determined by least-squares (non-linear) fitting of the experimental pairs H, t to the theoretical relations (13)–(17).

2.2.2. Calculation of time-resolved quantities of heterogeneous catalysts

These differ from the physicochemical quantities k_1, k_2, k_R and D_y of the previous Section 2.2.1, in that from the same chromatographic experiment a great number of values for the same physicochemical quantity can be calculated as a function of the measurement time, i.e., a time distribution of catalytic quantities. These can be attributed to different adsorption sites appearing active at different times and leading to different rates of adsorption–desorption, etc. The term "local" was used in the first such publication [5] meaning that not all adsorption sites are measurably active at the sampling time t. It is the nature of the RF-GC technique that permits such a discrimination.

The first such "local" quantities were adsorption energies, local monolayer capacities, and local isotherms [5,31], followed by probability density functions for adsorption energies [30,32], lateral molecular interactions on heterogeneous surfaces [41], surface energy on inert solids [37], and solid catalysts [38], surface diffusion coefficients [35], adsorption rates with lateral interactions [36]. A comparative article pointing out the interrelations between adsorption energies and local isotherms, local monolayer capacities, and energy distribution functions as determined by RF-GC is worth mentioning [24].

It is the feeling of the present author that this time separation of surface heterogeneity through experimental measurements of the quantities mentioned above is more important for heterogeneous catalysts as far as their kinetic properties are concerned, than overall values of rate constants, isotherms et al. determined by traditional gas chromatography. Therefore, a short description of the calculation methodology seems in order. The key starting point

is again Eq. (18), based on RF-GC and found by means of the PC program of Appendix A.

In most catalytic work by gas chromatography, the equilibrium constant of adsorption K plays an important role and is obtained from the net retention volume V_N of inverse gas chromatography experiments [6] usually referring to Henry's law pressures. In our work, however, a quite different approach was adopted starting from Eq. (10) of [5]:

$$\theta_t = \frac{c_s^*}{c_{max}^*} = 1 - \exp(-KRTc_y) \tag{21}$$

which is based on Jovanovic isotherm

$$\theta(p, T, \varepsilon) = 1 - \exp(-Kp) \tag{22}$$

In the above equations, θ_t or $\theta(p, T, \varepsilon)$ is the local adsorption isotherm on a heterogeneous surface, c_y and c_s^* have been defined after Eq. (6), c_{max}^* is the local monolayer capacity, K is the local Langmuir's constant and ε the local adsorption energy of the adsorbate. In order to avoid difficult integrations along the bed coordinate y, all above quantities can be taken at the one end $y = 0$ of the bed [5]. This does not change the conclusions, however, since they refer to the whole heterogeneous cross-sectional area a_y of the solid bed.

The calculation of KRT as a function of time from the experimental sample peaks H, t obtained by the RF-GC technique has been described in detail elsewhere [5,30,32]. The result, written in a convenient form is [30]:

$$KRT = \frac{gD_z}{vL_1}\left\{\frac{\sum_i A_i B_i^2 \exp(B_i t)}{\left[\sum_i A_i B_i \exp(B_i t)\right]^2} - \frac{1}{\sum_i A_i \exp(B_i t)}\right\} \tag{23}$$

where g, D_z, L_1 have been defined in Section 2.2, v is the corrected linear flow velocity of the carrier gas, and A_i, B_i are the parameters of Eq. (2) determined by the non-linear least-squares program of Appendix A.

From Eq. (22), as well as Eq. (23), one sees that Langmuir adsorption constant K has the units Pa^{-1}. Multiplying K by the gaseous standard state of 101 325 Pa (1 atm) and taking the logarithm multiplied by $-RT$, according to the relation:

$$\Delta G^\circ = -RT \ln K \tag{24}$$

one finds in a very simple way the value of ΔG° directly from the experimental data H, t of the RF-GC technique. Thus, ΔG° is a Langmuir quantity and not a Henry's law approximation, as usual [10]. Moreover, it corresponds to a specific experimental time and not to a scanning over the whole gas chromatographic band corresponding to all kinds of active sites of the heterogeneous solid surface. This gives a time distribution of surface energies.

From the same kind of experimental data H, t using calculations similar to Eq. (23) various other physicochemical quantities related to ΔG° have been determined in the same time-resolved way, e.g., adsorption energies [5], local monolayer capacities [5], local isotherms [5], and distribution functions of adsorption energy [30].

The relations used for these calculations are repeated here for convenience, namely, for the adsorption ε:

$$\varepsilon = RT \ln\left(\frac{K}{K^0}\right) \tag{25}$$

as derived from the Langmuir constant K found by Eq. (23) and its definition

$$K = K^0(T)\exp\left(\frac{\varepsilon}{RT}\right) \tag{26}$$

$K^0(T)$ is described by statistical mechanics [5] as

$$K^0 = \frac{h^3}{(2\pi m)^{3/2}(kT)^{5/2}}\frac{\upsilon_s(T)}{b_g(T)} \tag{27}$$

k being the Boltzman constant, m the molecular mass, h the Planck constant, $b_g(T)$ the partition function of the rotations and vibrations of the free gas molecule, and $\upsilon_s(T)$ the partition function of the adsorbed molecule over all possible quantum states. As a low temperature approximation, we adopt that $\upsilon_s(T) \approx b_g(T)$, as was done before [22].

Although the physical foundations of Eq. (22) have been criticized [42] this isotherm gives a good representation of experimental gas adsorption and behaves correctly at a wide range of surface coverages. An exhaustive numerical investigation of the differences in the behavior of the Jovanovic isotherm compared with that of Langmuir [43] led to the conclusion that, for the system krypton–pyrex, there is nothing to choose between the two and both give very similar values of the monolayer capacities. Also, Sircar [44] used the Jovanovic isotherm as the kernel $\theta(\varepsilon, T, p)$ in the integral Eq. (1) to calculate the energy distribution function $f(\varepsilon)$, and this resulted in the same form of $f(\varepsilon)$ as that obtained by using the Langmuir isotherm as the kernel. Only the variance of the calculated function was affected. Jaroniec et al. [45] investigated the possibility of extending the Jovanovic equation to multilayer adsorption on heterogeneous surfaces. In discussing numerical methods of evaluating the adsorption energy distribution from Eq. (1), Rudzinski and Everett [14] describe the application of Laplace transforms to the Jovanovic equation used as the local adsorption isotherm $\theta(p, T, \varepsilon)$, not only to monolayer but also to multilayer adsorption. Landman and Montroll [46] investigated the energy distribution function that converts the Langmuir local isotherm into the Jovanovic equation. The temperature dependence of this function shows that the picture of surface heterogeneity given by the Jovanovic and the Langmuir isotherms becomes more and more different as the temperature increases. The short review above regarding the Jovanovic isotherm [22] justifies its use to calculate adsorption energies of gases on solids by inverse GC in the form of RF-GC.

The fraction of the surface covered at a given time t is denoted by Eq. (21), c_{max}^* being now the local with respect to time monolayer capacity, i.e., the maximum adsorbed

concentration of the gaseous substance A on the collection of sites being active at time t and having a mean adsorption energy ε. Knowing KRT from Eq. (23) and c_y given by Eq. (4) of [5]:

$$c_y = \frac{\upsilon L_1}{gD_z}\sum_{i=1}^{3} A_i \exp(B_i t) \tag{28}$$

one easily calculates θ_t using Eq. (21). Then, c_s^* is found by means of Eq. (5) of [5]:

$$c_s^* = \frac{a_y}{a_s} k_1 \frac{\upsilon L_1}{gD_z}\sum_{i=1}^{3} \frac{A_i}{B_i}[\exp(B_i t) - 1] \tag{29}$$

and from $\theta_t = c_s^*/c_{max}^*$ of Eq. (21) c_{max}^* is computed.

Last but not least, the probability density function over time for the adsorption energy $f(\varepsilon)$ is quoted here from [30]:

$$f(\varepsilon; t) = \frac{\partial c_{max}^*}{\partial \varepsilon} = \frac{\partial c_{max}^*/\partial t}{\partial \varepsilon/\partial t} \tag{30}$$

as modified by Eq. (16) of [32]:

$$\phi(\varepsilon; t) = \frac{\theta_t f(\varepsilon; t)}{c_{max}^*} \tag{31}$$

where the adsorption energy ε is the random variable and the time t only a structural parameter. The other two quantities θ_t and c_{max}^* have just been defined by Eq. (21).

Calculating the numerator of Eq. (30) by differentiation of c_{max}^* with respect to time, and the denominator by differentiation of Eq. (25) with respect to time, one easily finds $f(\varepsilon; t)$, as:

$$f(\varepsilon; t) = \frac{1}{RT}\left[\frac{KRT(\partial c_s^*/\partial t) + (\partial^2 c_s^*/\partial c_y \partial t)}{\partial(KRT)/\partial t} - \frac{\partial c_s^*/\partial c_y}{KRT}\right] \tag{32}$$

All derivatives with respect to time in the above relation have been explicitly and analytically calculated from relations already given in [32] namely, $\partial c_s^*/\partial t$, $\partial^2 c_s^*/\partial c_y \partial t$, and $\partial c_s^*/\partial c_y$, and in [30] $\partial(KRT)/\partial t$.

Eq. (32) above was the central theme of publication [30] pointing out that $f(\varepsilon)$ is a function of two independent variables, ε and t, the t appearing as a structural parameter rather than a random variable of the distribution function. However, in a later publication [32] it was shown that the combination of $f(\varepsilon)$ with θ_t and c_{max}^*, as given in the form of Eq. (31) is a better choice for the true energy distribution function, behaving like a continuous probability density function for the variate ε and the structural parameter t, with respect to which can be normalized to unity by finding the value of the integral

$$\int_{t_1}^{t_2} \phi(\varepsilon; t)\mathrm{d}t = 1 \tag{33}$$

between the two limits t_1 and t_2 of the experimental time.

It must be pointed out that in all previous relations of this Section 2.2.2, based on the experimental function (2) or (18), the running index i = 1–3, for a reason explained elsewhere [35] and previously repeated at the beginning of Section 2.2 here.

Before going to other time-resolved quantities, it would be instructive to give some results for ε, c_{max}^*, θ_t and $f(\varepsilon; t)$ or $\phi(\varepsilon; t)$, all calculated from experimental measurements of the pairs H, t of Eq. (2) or Eq. (18). Table 1 of [5] gives typical results for ε, c_{max}^*, θ_t for two gases adsorbed on three solids. It is repeated here in Table 1.

Although the local relative coverage of the surface θ_t is known to be an increasing function of the equilibrium pressure or concentration and asymptotically tending to unity, the time dependence of the local θ_t is not necessarily analogous, since it does not comprise all sites, but only those active at time t. One can see from Table 1 that the maximum in ε and θ_t appears at the same time.

An evidence that the principles proposed here work is to calculate the local specific surface areas of the solid S (m^2/g) referring to each mean energy value ε_i (and therefore to each collection of active sites), by multiplying c_{max}^* by Avogadro's number, N_A, and by the molecular cross-sectional area of the adsorbed gas A_m. Using the liquid density of propene (0.5193) and Eq. (2.64) of Gregg and Sing's book [47], one finds for propene A_m = 28.58 Å^2. Then, $S = c_{max}^* N_A A_m \times 10^{-20}$ in m^2/g. Some values of S from the c_{max}^* values of Table 1 for C_3H_6/PbO, corresponding to a few chosen times, are given below:

t (min)	S (m^2/g)
6	0.015
18	0.086
28	0.298
42	1.20
50	6.59
52	47.9
54	10.9
60	3.31
120	3.86

Since PbO is a rather nonporous solid, the values S seem logical, distributed over the range 0.015–47.9 m^2/g, for the various collections of sites i.

In Fig. 4, the distribution function $\phi(\varepsilon; t)$ of Eq. (31) is plotted against the random variable of adsorption energy ε, and the structural parameter of time t. These two independent variables are closely connected through Eqs. (25) and (23). The main plot B in Fig. 4a corresponds to the middle period of time and has a Gaussian shape, the initial (A) and final (C) sections deviating very little from the middle (B). This is in sharp contrast to A, B and C curves of Fig. 4b, where ε has been replaced by t as independent variable. The three regions A, B and C are well separated, although energetically in (a) there is a very small or negligible separation. This is expected from the definition of Eq. (31), where $\phi(\varepsilon; t)$ is normalized with respect to the maximum capacity c_{max}^*

Table 1
Time distribution of adsorption energies (ε), local capacities (c^*_{max}), and local adsorption isotherm (θ_t) for two probe gases (C_2H_4, C_3H_6) and three solids (ZnO, PbO, $CaCO_3$) at 323.2 K[a]

Time (min)	ε(kJ/mol)				c^*_{max}(mol/g)				θ_t			
	C_2H_4		C_3H_6		C_2H_4		C_3H_6		C_2H_4		C_3H_6	
	ZnO	PbO	PbO	$CaCO_3$	ZnO	PbO	PbO	$CaCO_3$	ZnO	PbO	PbO	$CaCO_3$
6	88.3	88.4	88.8		1.18×10^{-6}	2.20×10^{-6}	8.68×10^{-8}		0.521	0.456	0.240	
8	90.9	89.7	89.6		1.72×10^{-6}	3.57×10^{-6}	1.87×10^{-7}		0.676	0.568	0.442	
10	96.6	91.7	90.7		2.03×10^{-6}	4.70×10^{-6}	2.84×10^{-7}		0.866	0.675	0.547	
12	97.1	95.0	92.2	89.4	2.69×10^{-6}	5.48×10^{-6}	3.67×10^{-7}	2.53×10^{-8}	0.877	0.801	0.638	0.144
14	91.0	106.2	94.4	88.9	4.28×10^{-6}	5.81×10^{-6}	4.29×10^{-7}	5.18×10^{-8}	0.690	0.970	0.738	0.266
16	88.1	96.6	98.4	88.6	6.42×10^{-6}	8.16×10^{-6}	4.66×10^{-7}	8.54×10^{-8}	0.551	0.844	0.861	0.332
18	86.0	92.4	109.4	88.6	9.43×10^{-6}	1.14×10^{-5}	4.97×10^{-7}	1.24×10^{-7}	0.434	0.710	0.980	0.382
20	84.3	90.1	97.2	88.7	1.40×10^{-5}	1.53×10^{-5}	6.87×10^{-7}	1.66×10^{-7}	0.332	0.610	0.836	0.426
22	82.7	88.5	93.8	89.0	2.15×10^{-5}	1.98×10^{-5}	8.98×10^{-7}	2.10×10^{-7}	0.239	0.532	0.731	0.468
24	81.0	87.2	91.7	89.4	3.58×10^{-5}	2.49×10^{-5}	1.14×10^{-6}	2.54×10^{-7}	0.157	0.469	0.648	0.509
26	78.9	86.2	90.2	89.9	7.11×10^{-5}	3.07×10^{-5}	1.42×10^{-6}	2.96×10^{-7}	0.085	0.417	0.580	0.550
28	75.3	85.4	89.0	90.5	2.53×10^{-4}	3.72×10^{-5}	1.73×10^{-6}	3.36×10^{-7}	0.026	0.373	0.521	0.592
30	74.6	84.6	88.0	91.2	3.29×10^{-4}	4.45×10^{-5}	2.09×10^{-6}	3.73×10^{-7}	0.021	0.334	0.468	0.636
32	77.0	84.0	87.1	92.1	1.40×10^{-4}	5.29×10^{-5}	2.52×10^{-6}	4.06×10^{-7}	0.052	0.300	0.420	0.683
34	77.8	83.3	86.2	93.2	1.07×10^{-4}	6.26×10^{-5}	3.03×10^{-6}	4.34×10^{-7}	0.072	0.269	0.373	0.733
36	78.1	82.7	85.5	94.7	9.56×10^{-5}	7.39×10^{-5}	3.66×10^{-6}	4.57×10^{-7}	0.084	0.240	0.329	0.788
38	78.2	82.1	84.7	96.8	9.23×10^{-5}	8.75×10^{-5}	4.46×10^{-6}	4.74×10^{-7}	0.090	0.213	0.286	0.850
40	78.2	81.6	83.9	100.3	9.31×10^{-5}	1.04×10^{-4}	5.51×10^{-6}	4.84×10^{-7}	0.093	0.187	0.243	0.920
42	78.2	81.0	83.1	119.2	9.64×10^{-5}	1.25×10^{-4}	6.98×10^{-6}	4.90×10^{-7}	0.093	0.162	0.202	0.998
44	78.0	80.3	82.2	100.1	1.02×10^{-4}	1.53×10^{-4}	9.15×10^{-6}	5.80×10^{-7}	0.090	0.138	0.161	0.917
46	77.8	79.7	81.2	96.6	1.09×10^{-4}	1.90×10^{-4}	1.27×10^{-5}	6.78×10^{-7}	0.087	0.115	0.121	0.847
48	77.6	78.9	79.9	94.6	1.19×10^{-4}	2.43×10^{-4}	1.96×10^{-5}	7.85×10^{-7}	0.082	0.093	0.081	0.787
50	77.3	78.1	78.0	93.1	1.30×10^{-4}	3.26×10^{-4}	3.83×10^{-5}	9.01×10^{-7}	0.077	0.071	0.043	0.732
52	77.0	77.0	72.6	92.0	1.44×10^{-4}	4.71×10^{-4}	2.78×10^{-4}	1.03×10^{-6}	0.071	0.051	0.006	0.684
54	76.7	75.6	76.6	91.1	1.61×10^{-4}	7.89×10^{-4}	6.35×10^{-5}	1.16×10^{-6}	0.065	0.031	0.028	0.639
56	76.4	73.0	78.5	90.3	1.81×10^{-4}	2.01×10^{-3}	3.24×10^{-5}	1.31×10^{-6}	0.059	0.12	0.056	0.598
58	76.0	70.4	79.4	89.6	2.06×10^{-4}	5.20×10^{-3}	2.34×10^{-5}	1.47×10^{-6}	0.052	0.005	0.080	0.560
60	75.7	74.2	80.0	89.0	2.37×10^{-4}	1.28×10^{-3}	1.92×10^{-5}	1.65×10^{-6}	0.046	0.020	0.100	0.524
64	74.8	76.4	80.7	87.9	3.25×10^{-4}	5.97×10^{-4}	1.54×10^{-5}	2.05×10^{-6}	0.035	0.046	0.130	0.460
68	73.7	77.3	81.1	86.9	4.81×10^{-4}	4.37×10^{-4}	1.39×10^{-5}	2.53×10^{-6}	0.024	0.065	0.151	0.402
72	72.3	77.7	81.3	86.1	8.14×10^{-4}	3.71×10^{-4}	1.32×10^{-5}	3.11×10^{-6}	0.015	0.079	0.166	0.349
76	69.9	78.0	81.4	85.3	1.95×10^{-3}	3.39×10^{-4}	1.30×10^{-5}	3.82×10^{-6}	0.006	0.088	0.174	0.302
78	67.4	78.1	81.4	84.9	4.98×10^{-3}	3.30×10^{-4}	1.30×10^{-5}	4.23×10^{-6}	0.002	0.092	0.177	0.281
80	64.9	78.2	81.4	84.6	1.22×10^{-2}	3.24×10^{-4}	1.31×10^{-5}	4.69×10^{-6}	0.001	0.095	0.179	0.260
82	68.7	78.2	81.4	84.2	2.98×10^{-3}	3.20×10^{-4}	1.32×10^{-5}	5.20×10^{-6}	0.004	0.097	0.180	0.241
84	70.1	78.2	81.4	83.9	1.78×10^{-3}	3.19×10^{-4}	1.34×10^{-5}	5.77×10^{-6}	0.007	0.098	0.180	0.222
90	71.9	78.2	81.2	82.9	9.13×10^{-4}	3.23×10^{-4}	1.41×10^{-5}	7.89×10^{-6}	0.14	0.010	0.177	0.174
98	72.9	78.0	81.0	81.6	6.47×10^{-4}	3.44×10^{-4}	1.56×10^{-5}	1.21×10^{-6}	0.020	0.097	0.168	0.123
100	73.0	78.0	80.9	81.3	6.16×10^{-4}	3.52×10^{-4}	1.60×10^{-5}	1.34×10^{-5}	0.021	0.095	0.165	0.112
106	73.3	77.7	80.6	80.4	5.61×10^{-4}	3.81×10^{-4}	1.76×10^{-5}	1.86×10^{-5}	0.024	0.090	0.155	0.085
110	73.4	77.6	80.4	79.8	5.42×10^{-4}	4.05×10^{-4}	1.88×10^{-5}	2.32×10^{-5}	0.025	0.085	0.148	0.070
120	73.4	77.1	79.9	78.3	5.31×10^{-4}	4.83×10^{-4}	2.24×10^{-5}	4.06×10^{-5}	0.026	0.073	0.128	0.043

[a] By permission from American Chemical Society.

of the sites and multiplied by their occupation factor θ. In spite of that, however, when $\phi(\varepsilon; t)$ is plotted against the experimental time t the three kinds of active sites are very well separated in time and their relative population is easily calculated by simply finding the three areas under the time curve of the three separate peaks.

Looking for a mechanism for the above experimental findings, one may compare the plots (b) of Fig. 4 with those three peaks of Fig. 5 in a relatively recent work [48], describing computer simulation of the adsorption of argon on titanium dioxide. Their peak with high adsorption energy was attributed to adsorption in the minimum of adsorption potential on the surface. The second peak with smaller energy was explained by assuming that it is not due to adsorption sites on a free surface, but to saddle points of adsorption potential surrounded by other tightly adsorbed species and providing support to molecules on those points. These places on the surface, where the total energy of an adsorbed molecule has a minimum are considered to become "new adsorption sites". Finally, their third peak with the smaller adsorption energy was explained as due to molecules very loosely bound to the substrate, in its second layer. The first adsorbed layer

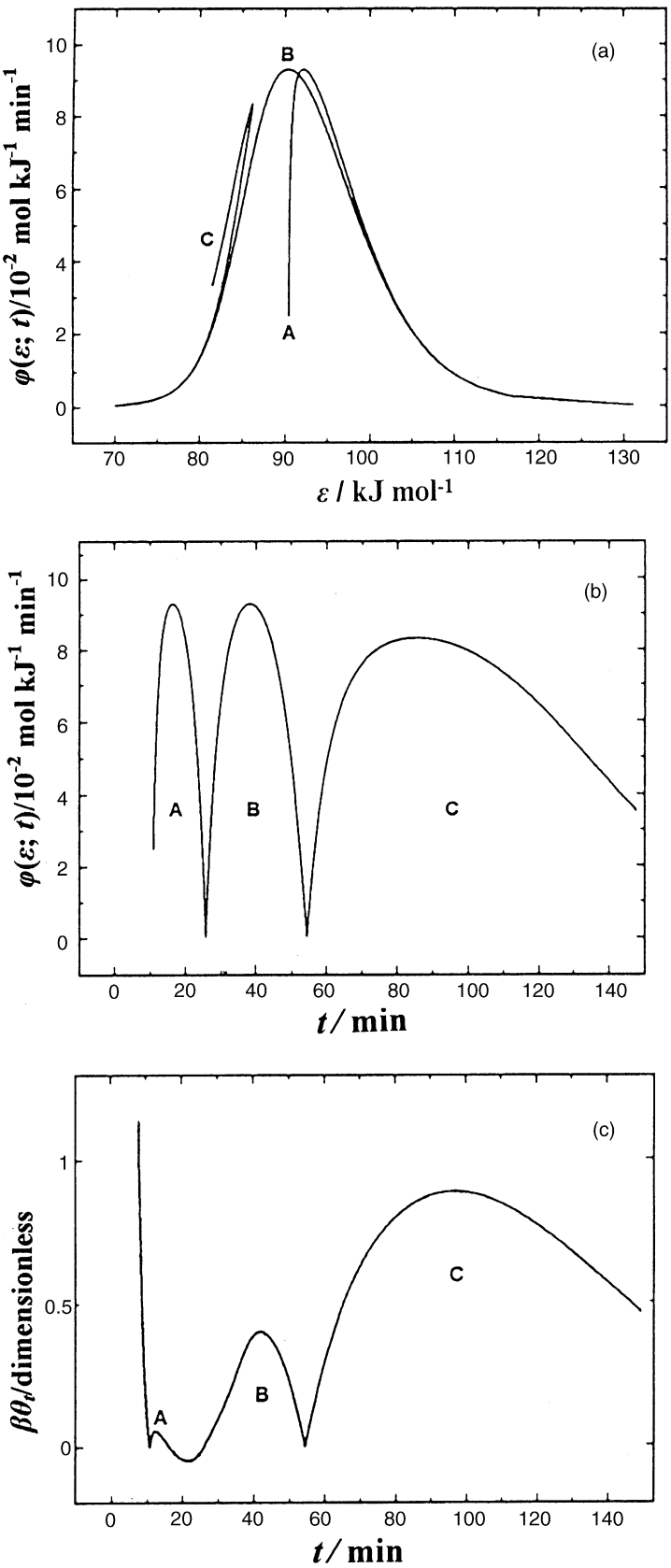

Fig. 4. Experimental behavior of the adsorption energy distribution function for the adsorption of 1-butene on cadmium sulphide, at 323.2 K. The distribution function $\phi(\varepsilon; t)$, as defined by Eq. (31) is plotted: (a) against the adsorption energy ε; (b) against the structural parameter of time t. In (c) the lateral molecular interaction energy $\beta\theta_t$ is plotted against time t.

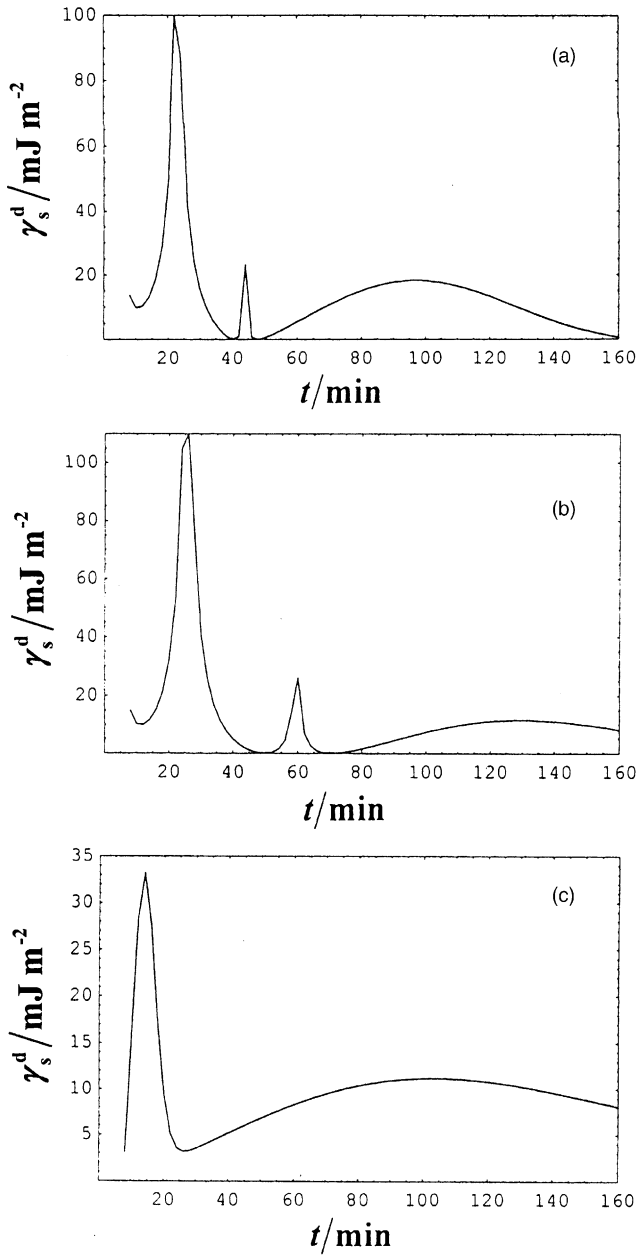

Fig. 5. Dispersive components of the total surface free energy γ_s^d of calcium oxide, plotted against time of measurement, as calculated by adsorption of: (a) pentane at 313.2 K; (b) hexane at 373.2 K; (c) heptane at 372 K.

is therefore not smooth but consists of molecules located at different distances from the surface. The adsorption in the second layer begins to grow when the first layer is almost totally completed. In contrast to the BET model, the surface of the monolayer which is already completed serves as a surface of adsorbent for the second layer.

The above mechanism of Bakaev and Steele [48] explains our results in Fig. 4b, although one could object to the comparison of our plots (b), being against time, with their Fig. 5 [48] plotted against adsorption energy. We do not think that this objection is justified, since the plot of Bakaev and Steele is based on purely computer simulation results of adsorption, obviously not taking into account the time parameter, whereas in Fig. 4 the structural experimental parameter t in $\phi(\varepsilon; t)$ plays a fundamental role for the separation of the three steps of the adsorption mechanism described above. How our second peak B, explained by assuming adsorption on new adsorption sites, could appear before these sites had been created by peak A due to adsorption in the minima of adsorption potential? And how our third peak C could show up as adsorption on the second layer before the completion of the first layer due to peaks A and B? Thus, the model mechanism of Bakaev and Steele seems to explain clearly our experimental findings, as those in Fig. 4 [49].

2.2.3. Lateral molecular interactions, surface diffusion, and adsorption rates on heterogeneous catalysts

These are some other time-resolved properties in addition to adsorption energy ε, local monolayer capacity c^*_{max}, local isotherm θ_t, and energy distribution function $f(\varepsilon)$, described in the previous subsection. As mentioned there, the second peak in Fig. 4b is explained by lateral molecular interactions creating new adsorption sites. These molecular interactions on heterogeneous surfaces can be found from the same experimental Eq. (2) or (18) by correcting Eq. (26) to include this type of energy:

$$K' = K^0 \exp\left(\frac{\varepsilon}{RT} + \beta\theta_t\right) = K \exp(\beta\theta_t) \tag{34}$$

where $\beta = z\omega/RT$ is a dimensionless parameter, ω denoting the lateral interaction energy and z the number of neighbors for each adsorption site. Thus, $z\omega\theta_t$ is the added to ε differential energy of adsorption due to lateral interactions.

Jovanovic isotherm (21) is modified accordingly, and from it a new derivative $\partial\theta_t/\partial c_y$ is calculated. Then, using this and some approximations, we reach the result:

$$\beta = \frac{1}{c_y}\left[\frac{\exp(KRTc_y) - 1}{KRT} - \frac{c_s^*}{\partial c_s^*/\partial c_y}\right] \tag{35}$$

in which all variables of the right-hand side are known as functions of time. Thus, β is easily calculated and the result is improved by some iterations [41].

In Fig. 4c, the lateral molecular interaction energy $\beta\theta_t$ (dimensionless), defined by Eq. (34) is plotted against the experimental time t. It is worth noting that the three maxima and the two minima in Fig. 4b almost coincide in time with the three maxima and the two minima of Fig. 4c. This points to a probable connection between them, adding a further support to the mechanism of Bakaev and Steele [48].

Another important kinetic property closely related to heterogeneous catalysis is surface diffusion coefficients for both reactants and products. It may involve physically adsorbed molecules, chemisorbed species, and self-diffusing atoms, ions, and clusters on the surfaces of their own crystal lattices. All three categories are important to catalysis.

Several techniques have been used to measure surface diffusion, the most common one for physically adsorbed and

chemisorbed species being the diffusion cell technique [50]. As stated in a recent review on surface diffusion [51], "any technique of monitoring local adsorbate concentrations can be used to measure surface diffusion". However, Smith [52] states "Experimental verification of surface diffusion is usually indirect, since concentrations of adsorbed molecules on a surface are difficult to measure. When gas concentrations are obtained, the problem arises of separating the surface and pore volume transport rates". Radioactive labeled adsorbates, infrared and electron spectroscopies, low energy electron diffraction, field emission microscopy (FEM) and field ion microscopy (FIM) enabled the observation of migration of individual adatoms, but these techniques have been limited to refractory metals, mostly to tungsten surfaces. They are not applicable, however, to studying surface diffusion of physically or chemisorbed species.

According to Jaroniec and Madey [23], in the majority of papers concerning adsorption kinetics on solids, the models of mass-transfer kinetics (involving external, internal, and surface diffusion of adsorbate molecules) were studied. According to Eq. (5.3) of [23]:

$$D_i = D_0 + D_s \frac{\partial \theta}{\partial p} \tag{36}$$

that is, the diffusion coefficient is divided into two parts: the term D_0 describing diffusion in the bulk phase, and the second term referring to the diffusion in the surface phase. The pressure p reflects the concentration of the adsorbate in the bulk phase, and the adsorption isotherm θ reflects the concentration of the adsorbate in the surface phase. The surface diffusion coefficient D_s in Eq. (36) is the physicochemical quantity sought and this can be easily calculated, since all other quantities in this equation are either known physical properties, or can be obtained quite easily from the pairs H, t of the RF-GC experiments, as follows. The total diffusion coefficient D_i should be equal to $D_z\varepsilon_M^2$, i.e., to that of the adsorbate in the carrier gas in the absence of solid D_z, multiplied by the square of the macro void fraction in the bed ε_M, according to the random-pore model ([52], p. 467). This is required for boundary condition reasons at $z = L_1$, $y = 0$. The D_0 term of Eq. (36) is equal to the experimental D_y, calculated from the H, t pairs as described in Section 2.2.1 together with the rate constants.

There remains the partial derivative $\partial\theta/\partial p$ of Eq. (36) to be found. This is most easily done from Eq. (22) where K is Langmuir's constant given by Eq. (26) and K^0 being given by Eq. (27). Taking the partial derivative of θ with respect to p in Eq. (22) one simply finds:

$$\frac{\partial \theta}{\partial p} = K \exp(-Kp) = K(1-\theta) \tag{37}$$

and, substituting in it Eq. (26) for K, there results

$$\frac{\partial \theta}{\partial p} = K^0(1-\theta)\exp\left(\frac{\varepsilon}{RT}\right) \tag{38}$$

All three factors on the right-hand sides of Eqs. (37) and (38) above are easily calculated, namely, K by Eq. (23), K^0 by Eq. (27), θ by Eq. (21) and ε or ε/RT by Eq. (25). Except for K^0, all other quantities are found from the values of A_1^0, A_2^0, A_3^0, B_1, B_2, B_3, of Eq. (18), and the time parameter t. Thus, $\partial\theta/\partial p$ is found with a time-resolved procedure from the experimental chromatographic data H, t of the RF-GC method. Finally, the relation giving D_s is easily obtained from Eq. (36):

$$D_s = \frac{D_z\varepsilon_M^2 - D_y}{\partial\theta/\partial p} = \frac{D_z\varepsilon_M^2 - D_y}{K^0(1-\theta)}\exp\left(-\frac{\varepsilon}{RT}\right) \tag{39}$$

It is worth noticing that this equation coincides in form with the equation of Higashi et al. [53]:

$$D_s = \frac{D_{s0}}{1-\theta}\exp\left(-\frac{E}{RT}\right) \tag{40}$$

if $D_{s0} = (D_z\varepsilon_M^2 - D_y)/K^0$ and adsorption energy ε behaves like the activation energy E of the surface diffusion process.

All calculations described can be carried out simultaneously by the GW-BASIC personal computer program listed in Appendix A, by entering the H, t pairs in the DATA lines 3000–3040, together with some auxiliary physical quantities, in the INPUT lines.

The methodology and calculations described here are demonstrated by their application to the adsorption of carbon monoxide, oxygen gas and carbon dioxide on a platinum–rhodium alloy catalyst containing 75% Pt + 25% Rh supported on SiO_2 (3% w/w), at a temperature of 593.8 K [35].

Thus, with a very simple modification of a commercial gas chromatograph, one can measure in a single experiment the surface diffusion coefficient in a time-resolved way, combined with a simultaneous measurement of the adsorption energy, the local adsorbed concentration, and the local adsorption isotherm, for gaseous adsorbates on heterogeneous solid surfaces, as described in Section 2.2.2.

The same data used so far can be employed to calculate the net adsorption rate as a function of time with lateral molecular interactions, together with the rate constants of adsorption k_a (min^{-1}) and desorption k_d (min^{-1}). One can start from Eq. (21) which is based on Jovanovic isotherm (22). Differentiating Eq. (21) with respect to time, one obtains the rate of change of θ_t, i.e., the net adsorption rate:

$$\frac{\partial \theta_t}{\partial t} = \left[KRT\frac{\partial c_y}{\partial t} + c_y\frac{\partial(KRT)}{\partial t}\right]\exp(-KRTc_y) \tag{41}$$

The various functions and the derivatives on the right-hand side of the above can be obtained from Eq. (28) for c_y, Eq. (23) for KRT and Eq. (15) of [30] for $\partial(KRT)/\partial t$, respectively, and the following relation for $\partial c_y/\partial t$:

$$\frac{\partial c_y}{\partial t} = \frac{\upsilon L_1}{gD_z}\sum_{i=1}^{3} A_i B_i \exp(B_i t) \tag{42}$$

Naturally, the present function (18) with i = 1–3 is used in all above calculations.

If the $\partial\theta_t/\partial t$ value, calculated by Eq. (41) above, represents the local net adsorption rate, it can be written in a way analogous to Eqs. (5–22) of Jaroniec and Madey [23]:

$$\frac{\partial\theta_t}{\partial t} = k_a c_y RT(1-\theta_t) - k_d\theta_t \exp(-\beta\theta_t) \quad (43)$$

thus showing the explicit dependence of the net adsorption rate on the local surface coverage θ_t of a heterogeneous surface, as previously assumed [5,24,30–32]. In the above relation, $\partial\theta_t/\partial t$ is found from Eq. (41), θ_t can be found directly by Eq. (22), c_y from Eq. (28), and β is the lateral interaction parameter (dimensionless) of Eq. (35). Setting $K = k_a/k_d$, according to microscopic reversibility, K being calculated from the KRT value, the only unknown in Eq. (43) is k_a. Thus, both rate constants, k_a and k_d, can be found as functions of time, and of θ_t.

All above calculations are incorporated into the PC program of the Appendix A, together with the calculation of the other previous kinetic properties.

The calculations described above have been applied to two systems, as examples, namely, the adsorption of dimethyl sulfide on pieces of marble, and the adsorption of heptane on γ-alumina, both at temperatures higher than the boiling points of the adsorbates, under atmospheric pressure [36]. From the results obtained, some general conclusions can be drawn. There is certainly a time-resolved heterogeneity of the solid surfaces manifesting itself in all calculated physicochemical parameters. The smallest variation appears in the adsorption energy showing a maximum at 85–100 min for $(CH_3)_2S$/marble, and at 260–280 min for n-C_7H_{16}/γ-alumina. The energy distribution function shows more than one maxima, as before [32].

The variation of the local isotherm θ_t with time shows an increasing up to almost unity with time (adsorption period), and then decreasing slowly to much smaller values (desorption period). The main objective of the work [36] was the experimental variation of adsorption rates and relative rate constants with local surface coverage. It is clear that $\partial\theta_t/\partial t$ decreases with increasing θ_t, as expected, to a negligible value at $\theta_t \approx 1$, and then increases again with decreasing θ_t obviously due to desorption. It passes through a maximum and then it decreases slowly. This behavior, which is predicted theoretically by Eq. (43), has never been measured experimentally before, as far as I know.

3. Typical recent results with platinum–rhodium alloy catalysts for the oxidation of CO to CO_2

The methodology of RF-GC to study heterogeneous catalysis in conjunction with surface science aspects is exemplified by the recent studies of carbon monoxide oxidation over Pt-Rh alloy catalysts, which is very important for the control of automotive emissions. First, the mechanism of CO oxidation was formulated from the adsorption of CO, O_2 and CO_2, by determining the rate constants, k_1, k_2 and k_R of Section 2.2, as well as their Arrhenius dependence on temperature [54]. Then, a partial dissociative adsorption of CO was detected followed by reaction of the adsorbed CO with adsorbed O atoms, the conclusions being based on activation energy calculations [55].

Catalytic fractional conversions of CO to CO_2 over the above catalysts, in the presence of excess O_2, under steady-state or non steady-state conditions were measured by the RF-GC technique [56]. Activation energies were also determined, which depended on the catalyst Pt content.

In another work [57], CO adsorption was found to be a dissociative process with a beneficial Pt-Rh synergism.

A tool for instantaneous monitoring of the reactants and products concentrations in heterogeneous catalytic processes is offered by RF-GC [58]. Conversion as a function of time can be compared to that of steady-state.

Time distribution properties, like those of Section 2.2.2, namely, adsorption energies, local monolayer capacities, local isotherms et al. have been measured for silica supported 25% Pt + 75% Rh catalyst [59].

Finally, the adsorption of CO on a silica supported rhodium catalyst, referring to a wide range of hydrogen rich atmosphere (25–75% H_2), under experimental conditions compatible with the operation of fuel-cells [60] lead to the conclusion that RF-GC gives similar results with those obtained by other techniques.

4. Chemical kinetic properties and surface energy of catalysts

Accepting what has been written in the Introduction, that gas chromatography is a promising meeting place of surface science and heterogeneous catalysis, one cannot ignore an important physicochemical quantity of solid surfaces, i.e., surface energy.

As described by Voelkel in a wonderful review pertaining to inverse gas chromatography [61], intermolecular interactions in adsorbent/adsorbate system may be dispersive and specific which corresponds to the dispersive (γ_s^d) and specific component (γ_s^s) of free surface energy (γ_s) of adsorbend:

$$\gamma_s = \gamma_s^d + \gamma_s^s \quad (44)$$

The standard free energy ΔG° for transferring a mol of vapor from the gas phase to a standard state of the surface is

$$\Delta G^\circ = -RT \ln \frac{BV_N}{Sm} \quad (45)$$

where B is the coefficient according to DeBoer's definition of the surface pressure in the adsorbed state, S is the specific area of adsorbent, m its mass within the column, and V_N the net retention volume. For a given system B, S, and m are constants and Eq. (45) changes into:

$$\Delta G^\circ = -RT \ln V_N + \text{const.} \quad (46)$$

For the test substance, ΔG° is the sum of adsorption energies attributed to dispersive ΔG^d and specific ΔG^s interactions:

$$\Delta G^\circ = \Delta G^d + \Delta G^s \quad (47)$$

For *n*-alkanes $\Delta G^\circ = \Delta G^d$ and changes with the number of carbon atoms in the molecule. The increment of adsorption energy corresponding to methylene group CH_2 may be found from:

$$\Delta G_{CH_2} = -RT \ln \left(\frac{V_{N,n}}{V_{N,n+1}} \right) \quad (48)$$

where $V_{N,n}$ and $V_{N,n+1}$ denote the net retention volumes of two consecutive *n*-alkanes with n and $n+1$ carbon atoms in the molecule. According to Dorris and Gray [62]:

$$\Delta G_{CH_2} = 6.023 \times 10^{23} a_{CH_2} 2(\gamma_s^d \gamma_{CH_2})^{1/2} \quad (49)$$

where a_{CH_2} denotes the surface covered by one methylene group ($0.06\,nm^2$) and γ_{CH_2} is the free surface energy of polyethylene, most often being taken as $35.6\,mJ/m^2$.

The approximation expressed by the last factor of Eq. (49) above was generalized by Dorris and Gray [10], adopting a suggestion of Fowkes [63], that the work of adhesion between a saturated hydrocarbon and a second phase is given by the geometric mean of the dispersive components of the surface free energies of cohesion $2\gamma^d$ of the two pure phases:

$$W_A = 2(\gamma_1^d \gamma_2^d)^{1/2} \quad (50)$$

According to Fowkes, γ_1^d is equal to the surface tension of the saturated hydrocarbon, while γ_2^d is the dispersive part of the total surface free energy of the solid.

In a more recent work, Nardin and Papirer [11] propose the use of the vapor pressure of the adsorbate as additional means to extract γ_2^d from the chromatographic data. Later work of Bogillo and Voelkel [64] using the traditional IGC instrumentation found that modification of the rutile surface by sequential coating with amorphous alumina and silica patches leads to an increase of the dispersive component of the surface free energy. They explained this effect in terms of the contribution of the highly polarized alumina patches to the surface free energy of the mixed oxide.

In Part 2 of the same series of papers, Bogillo et al. [65] examined the characteristics of the water/solid interface by means of ^1H NMR spectroscopy with bulk freezing, and deduced that the surface modification of rutile leads to an increase of the excess Gibbs energy of water at the interface as well as of the thickness of the water film.

In another work, Voelkel et al. [66] approached the calculation of the adsorption free energy and its distribution on a heterogeneous solid surface as the sum of two uniform functions found directly from co-ordinates of the tail of the probe's chromatographic peak.

Even latest work like that of Hamieh et al. [12] or those presented at the 1st International Conference on IGC [67] have not abandoned the net retention volume V_N as the main source of chromatographic information for surface energy calculations, frequently at infinite dilution. Of course there are other recent works based on quite different experimental approach, as reflection absorption infrared spectroscopy, used with mixed adsorbate systems [68].

When one deals with high energy systems, the calculation of the value of γ_2^d of Eq. (50) can be based, not only on the surface tension of the saturated hydrocarbons, but to a completely different way from usual for calculating the fundamental quantity of adsorption free energy ΔG°. Instead of the net retention volume V_N of classical IGC [cf. Eq. (45)], the local adsorption energies, the local isotherms, and the local monolayer capacities on heterogeneous surfaces [5], as well as the relevant distribution functions [30,32] from RF-GC can be employed, all applied to heterogeneous solid surfaces, without any connection pertaining to classical gas–solid chromatography.

The experimental set-up of the RF-GC method described in paragraph 1 (Fig. 3) can be used, and Eq. (2) or Eq. (18) may be employed for analysing the experimental series of *H*, *t* pairs, so that Eq. (23) is found. Eq. (24) follows from it, instead of Eq. (45), pertaining directly to experimental data. It should be repeated here that this *K* value corresponds to a specific experimental time and not to a scanning over the whole gas chromatographic band corresponding to all kinds of active sites of the heterogeneous solid surface. This gives a time distribution of surface energies.

According to literature [62,64,66], for non-polar probes $-\Delta G^\circ = N_A a W_A$, where N_A is Avogadro number, a is the surface area per adsorbed molecule, and W_A is given by Eq. (50). Thus:

$$-\Delta G^\circ = 2N_A a(\gamma_h^d \gamma_s^d)^{1/2} \quad (51)$$

where index 'h' refers to a saturated hydrocarbon and 's' to the solid surface. Since ΔG° can be determined by Eq. (24) with the help of Eq. (23) and N_A is a known number, there remain a and γ_h^d for the hydrocarbons used to find γ_s^d for the solid surface. As regards a the molecular cross-sectional area of the adsorbed hydrocarbons can be used, calculated from their liquid density and Eq. (2.64) of Gregg and Sing's book [47]. It can be found $0.3622\,nm^2$ for pentane, $0.3936\,nm^2$ for hexane, and $0.4253\,nm^2$ for heptane [37]. The γ_h^d was taken equal to the surface tension of each hydrocarbon at the temperature of the experiment, as postulated by Fowkes [63]. The surface tensions were calculated by Eq. (3-63) of [69] at the appropriate temperature. Naturally, all calculations are based on Jovanovic isotherm, and may not be applicable to alkanes at elevated partial pressures, where their isotherms are rather of type II.

From the same kind of experimental data *H*, *t* using calculations similar to Eq. (23), the probability density function over time can be found for the dispersive part of the surface free energy of the solid γ_s^d. This can be done in a way analogous to that used for the distribution of the total adsorption energy, namely, Eq. (30) as modified by Eq. (31), where the adsorption energy ε was the random variable and the time t only a structural parameter.

Table 2
Adsorption energies, (ε), free energies of adsorption (ΔG°), local adsorbed concentrations (c_s^*), local adsorption isotherms (θ_t), total surface free energies (γ_s^d), and probability density functions [$\phi(\gamma_s^d;\ t)$] of (γ_s^d) for chosen values of the structural parameter t, all for the adsorption of pentane, hexane and heptane on silica gel at 373.2 K[a]

Time (min)	ε (kJ/mol)	ΔG° (kJ/mol)	c_s^* (μmol/g)	θ_t	γ_s^d (mJ/m^2)	$100\,\phi(\gamma_s^d;\ t)$ (m^2/mJ)
Pentane						
10	84.07	8.18	4.15	0.105	18.3	0.0431
28	89.52	0.729	8.68	0.289	0.254	2.93
30	89.99	0.255	9.03	0.311	0.0312	9.24
32	90.45	−0.203	9.36	0.333	0.0197	12.7
34	90.89	−0.645	9.67	0.356	0.200	4.31
36	91.32	−1.07	9.96	0.379	0.522	2.77
88	97.32	−7.08	14.27	0.699	24.0	4.98
90	97.34	−7.10	14.37	0.693	24.1	11.03
92	97.35	−7.11	14.47	0.686	24.2	218.3
94	97.34	−7.10	14.56	0.677	24.1	12.2
96	97.32	−7.08	14.66	0.666	24.0	4.93
Hexane						
10	83.05	8.02	38.12	0.0945	21.8	0.193
16	88.17	2.90	45.28	0.212	2.85	1.41
18	89.75	1.32	46.70	0.269	0.593	3.95
20	91.25	−0.175	47.83	0.335	0.0104	36.70
22	92.65	−1.58	48.75	0.409	0.848	4.79
24	93.96	−2.89	49.51	0.487	2.82	2.96
36	98.88	−7.80	52.33	0.797	20.64	0.132
38	99.09	−8.02	52.66	0.796	21.7	2.49
40	99.10	−8.03	52.96	0.776	21.8	3.27
42	98.91	−7.84	53.25	0.734	20.8	0.578
44	98.52	−7.45	53.52	0.669	18.8	1.41
56	88.54	2.53	54.89	0.0326	2.17	0.591
58	89.00	2.07	55.07	0.0360	1.46	0.785
60	91.71	−0.634	55.26	0.0804	0.136	5.20
62	92.79	−1.72	55.44	0.107	1.01	2.23
64	93.37	−2.30	55.60	0.123	1.80	1.51
68	93.88	−2.81	55.92	0.131	2.68	0.462
70	93.97	−2.90	56.06	0.128	2.85	4.15
72	94.00	−2.92	56.20	0.124	2.89	77.2
74	93.97	−2.90	56.33	0.117	2.84	4.85
Heptane						
20	94.65	−2.88	1.434	0.751	2.14	1.90
22	93.68	−1.91	1.558	0.615	0.941	4.16
24	92.81	−1.04	1.673	0.492	0.279	8.27
26	91.99	−0.212	1.781	0.384	0.012	40.1
28	91.14	0.633	1.883	0.291	0.103	12.7
30	90.20	1.57	1.977	0.211	0.637	4.61
34	87.28	4.50	2.146	0.0764	5.22	0.866
36	82.92	8.85	2.221	0.0180	20.2	0.121
38	85.32	6.45	2.291	0.0359	10.7	0.317
40	88.24	3.53	2.356	0.0830	3.22	1.18
114	103.4	−11.7	3.307	0.901	35.1	2.94
116	103.5	−11.7	3.320	0.899	35.3	9.07
118	103.5	−11.7	3.332	0.895	35.3	18.7
120	103.4	−11.7	3.344	0.891	35.2	3.74
122	103.4	−11.6	3.356	0.885	35.0	1.56

[a] By permission from Colloid and Surfaces A.

One may adopt a definition for $f(\gamma_s^d;\ t)$ similar to that of Eq. (30):

$$f(\gamma_s^d;\ t) = \frac{\partial c^*_{max}}{\partial \gamma_s^d} = \frac{\partial c^*_{max}/\partial t}{\partial \gamma_s^d/\partial t} \tag{52}$$

and then, as in Eq. (31)

$$\phi(\gamma_s^d;\ t) = \frac{\theta_t f(\gamma_s^d;\ t)}{c^*_{max}} \tag{53}$$

First, θ_t can be calculated from Eq. (21), since KRT can be found by using Eq. (23) and c_y by Eq. (28). Then, c_s^* is given by Eq. (29) k_1 having been calculated as described in Section 2.2.1. From Eq. (21) one obtains:

$$c^*_{\max} = \frac{c^*_s}{\theta_t} \tag{54}$$

Going back to the calculation of the distribution functions of γ^d_s by means of Eqs. (52) and (53), the derivative $\partial c^*_{\max}/\partial t$ is easily found by differentiating with respect to time Eq. (54):

$$\frac{\partial c^*_{\max}}{\partial t} = \frac{\theta_t(\partial c^*_s/\partial t) - c^*_s(\partial\theta_t/\partial t)}{\theta_t^2} \tag{55}$$

$\partial c^*_s/\partial t$ and $\partial\theta_t/\partial t$ being taken by differentiating with respect to time Eqs. (29) and (21), respectively. As to the derivative $\partial\gamma^d_s/\partial t$ needed in Eq. (52), this can be obtained by differentiating Eq. (51) with respect to time and rearrangement:

$$\frac{\partial\gamma^d_s}{\partial t} = -\frac{1000\partial(\Delta G^\circ)/\partial t}{N_A a\gamma^d_h}(\gamma^d_h\gamma^d_s)^{1/2} \tag{56}$$

the factor 1000 changing the units of ΔG° from J/mol to mJ/mol and a being expressed in m^2.

In Fig. 5, the dispersive component of the total surface free energy γ^d_s is plotted against the time of measurement for the solid surface of calcium oxide, derived from the adsorption of three saturated hydrocarbons (pentane, hexane and heptane), as recently published [37].

It is difficult to explain the variation of γ^d_s with time as depicted in Fig. 5, but all quantities mentioned before change with the observation time. An obvious explanation for these changes has already being given in the first publication of this kind [5], as due to the heterogeneity of the solid surface regarding adsorption energy ε_i, local adsorption isotherm θ_t, and local monolayer capacity $c^*_{\max}$. Fig. 2 of that work shows the experimental sweeping effect of time on these variables all of which refer to a single cross-section of the solid bed at $y = 0$, as mentioned before. All values refer to a time period $0 - t$, and not to a single t value, as is obvious from Eq. (8). Therefore, they are transition values over various active sites, before being leveling off with time. The phenomenon does not appear in traditional IGC, since the net retention volumes V_N calculated in it represent weighed mean values effected by the traditional broadening factors of elution chromatography.

In Table 2, the values of ε_i, ΔG°, c^*_s and θ_t are given, corresponding to the extreme values (maxima and minima) of γ^d_s. Some values preceeding and following the extremes are also given, together with the respective probability density functions of Eq. (53).

It is clear from Table 2 that there is no apparent correlation of γ^d_s with the local adsorbed equilibrium concentrations c^*_s and the degree of surface coverage θ_t. The maxima and minima in γ^d_s are, however, closely connected to their probability density function $\phi(\gamma^d_s; t)$, which incorporates $c^*_{\max}$ and θ_t, according to Eq. (53). Also, there is no correlation of γ^d_s with the rate of adsorption $\partial\theta_t/\partial t$, not given in the Table for this reason.

If one calculates the mean value of γ^d_s in the whole time period of the measurements, taking into account the respective values of the distribution function $\phi(\gamma^d_s; t)$, he does not find the same mean value with all three saturated hydrocarbons using the same solid surface. For example, at 373.2 K the three systems pentane/silica gel, hexane/silica gel, and heptane/silica gel give 19.62, 3.44 and 9.15 mJ/m^2, respectively, for $\langle\gamma^d_s\rangle$. The mean total free energy of adsorption $\langle\Delta G^\circ\rangle$ was found −6.79, −3.66, and −9.08 kJ/mol, respectively, for the same above systems.

For the CaO solid surface, the $\langle\gamma^d_s\rangle$ values found were 10.65, 9.29, 10.66 mJ/m^2 with pentane, hexane and heptane, respectively, while the $\langle\Delta G^\circ\rangle$ values were −6.13, −5.76, −6.47 kJ/mol, respectively. These findings are obviously in disagreement with Fowkes formalism, according to which the work of adhesion between a saturated hydrocarbon and a solid phase is solely due to London dispersion forces. At least this has not been found to hold here for the entire region of experimental time. If, however, one calculates the mean values within the last time period corresponding to the last Gaussian bands (cf. Fig. 5), the results do not differ very much from one hydrocarbon to the other. For example, the $\langle\gamma^d_s\rangle$ values for the systems C_5H_{12}/CaO, C_6H_{14}/CaO, and C_7H_{16}/CaO gave for $\langle\gamma^d_s\rangle$ 9.70, 9.52, and 10.96 mJ/m^2, respectively, whereas $\langle\Delta G^\circ\rangle$ ranged as −6.08, −5.59, and −6.52 kJ/mol. According to a previous work [32], the last broad Gaussian bands obtained by the RF-GC method correspond to loosely bound adsorbate molecules on the second layer of the solid surfaces.

Acknowledgements

The excellent typescript preparation is attributed to Miss Anna Malliori, for which the author is deeply obliged.

Appendix A. GW-BASIC programme for some calculations mentioned in the present review.

```
10 REM Calculation of Ai and Bi parameters of Eq.(2), together with

       the surface energy properties
20 REM Non-Linear Regression Analysis of Function:
30 REM H^(1/M)=A5*EXP(B5*T)+S*A6*EXP(B6*T)+P*A7*EXP(B7)
40 REM N2     = Minimum number of points of first exponential function
50 REM MAX    = Square of maximum correlation coefficient
60 REM OPT    = Final optional choice of variables when OPT=1
70 REM J      = Number of points of first exponential function
80 REM G      = Number of points of second exponential function
90 REM F    = Number of points of third exponential function
100 LPRINT
110 REM SA,SB = Standard errors of A and B in each linear regression
120 REM Y(I)  = Ordinate for each linear regression in the subroutine
130 REM U(I)= Variable remaining by  removal of the previous one,or two

             exponential functions
140 REM D(I)= Function for calculating the squared correlation coefficient
150 CLEAR ,,10000
160 INPUT "Maximum number of pairs H,T=";NF
170 INPUT "Minimum number of pairs H,T=";NS
180 DIM H(NF),T(NF),Y(NF),U(NF),D(NF)
190 INPUT "Response factor=";M
200 INPUT "Factor to divide H(I)=";H1
210 INPUT "Temperature in K=";T0
220 INPUT "Lenth L1(cm) of Section z=";L1
230 INPUT "Length L2(cm) of Section y=";L2
240 INPUT "External Porosity E of the Solid bed=";E
250 INPUT "Cross sectional area Az(cm^2) of Empty Section L1 =";AZ
260 INPUT "Cross Sectional Area Ay(cm^2) of Filled Section L2=";AY
270 INPUT "Amount of Adsorbent per Unit Length of Bed AS(g/cm)=";AS
280 INPUT "Cross Sectional Area of Adsorbate in A^2=";CSA
290 INPUT "Volumetric Flow-rate of Carrier Gas V'(cm^3/min)=";V0
300 INPUT " Negative Molecular Diffusion Coefficient in the Gas (cm^2/s)=";D1
305 INPUT " Molar mass MB(kg/mol) of the Analyte ="; MB
310 INPUT "Amount of Reactant injected NB(mol)=";NB
320 INPUT "Linear Flow-velocity of Carrier Gas(cm/s)=";LV
330 INPUT "Surface Tension of Adsorbate in dynes/cm=";ST
333 INPUT "Initial Time in min=";T1
336 INPUT "Final Time in min=";T2
340   FOR I=1 TO NF
350    READ H(I),T(I)
360    H(I)=H(I)/H1
370   NEXT I
380 MAX=0:OPT=0
390 FOR N=NF TO NS STEP -1
400 N2=INT(N/6+.5)
410  REM Calculation of A5 and B5 with H,T pairs ranging from N2 to N-N2-3
420 FOR J=N2 TO N-N2-3
430    K=N-J+1
440    L=N
450    FOR I=K TO L
460       Y(I)=(1/M)*LOG(H(I))
470    NEXT I
480    GOSUB 4000        : REM Subroutine for linear regression analysis
490    A5=EXP(A)
500    B5=B
510    SA5=SA
520    SB5=SB
530    IF OPT=1 THEN  570
540  REM Calculation of A6 and B6 with H,T pairs ranging from N2 to N-J-3

        and both prefixes -1 and +1
550    FOR S=-1 TO +1  STEP 2
560       FOR G=N2 TO N-J-3
570          K=N-J-G+1
580          L=N-J
```

Appendix A. (*Continued*)

```
590          FOR I=K TO L
600             U(I)=S*H(I)^(1/M)-S*A5*EXP(B5*T(I))
610             Y(I)=LOG(ABS(U(I)))
620          NEXT I
630          GOSUB 4000     : REM Subroutine for linear regression analysis
640          A6=EXP(A)
650          B6=B
660          SA6=SA
670          SB6=SB
680          IF OPT=1 THEN 710
690  REM Calculation of A7 and B7 with H,T pairs ranging from 1 to N-J-G,

         with both prefixes -1 and +1
700          FOR P=-1 TO +1 STEP 2
710             K=1
720             L=N-J-G
730             FOR I=K TO L
740                U(I)=P*(H(I)^(1/M)-A5*EXP(B5*T(I))-S*A6*EXP(B6*T(I)))
750                Y(I)=LOG(ABS(U(I)))
760             NEXT I
770          GOSUB 4000  : REM Subroutine for linear regression analysis
780             A7=EXP(A)
790             B7=B
800             SA7=SA
810             SB7=SB
820             IF OPT=1 THEN 1020
830             C1=0
840             C2=0
850             C3=0
860             FOR I=1 TO N
870                D(I)=H(I)^(1/M)-A5*EXP(B5*T(I))-S*A6*EXP(B6*T(I))

                        -P*A7*EXP(B7*T(I))
880                C1=C1+D(I)^2
890                C2=C2+H(I)^(2/M)
900                C3=C3+H(I)^(1/M)
910             NEXT I
920             R=1-C1/(C2-C3^2/N)
930             IF R>MAX THEN MAX=R:SMAX=S:PMAX=P:JMAX=J:GMAX=G:NMAX=N
940 PRINT MAX
950          NEXT P
960       NEXT G
970    NEXT S
980 NEXT J
990 NEXT N
1000 S=SMAX:P=PMAX:J=JMAX:G=GMAX:N=NMAX:OPT=1
1010 GOTO 430
1020 LPRINT "Intercept Ln(A5) and its Standard error=";LOG(A5*H1) "+-"SA5
1030 LPRINT "Slope B5 and its Standard error=";B5 "+-"SB5
1040 LPRINT
1050 LPRINT "Intercept Ln(A6) and its Standard error=";LOG(A6*H1) "+-"SA6
1060 LPRINT "Slope B6 and its Standard error=";B6 "+-"SB6
1070 LPRINT
1080 LPRINT "Intercept Ln(A7) and its Standard error=";LOG(A7*H1) "+-"SA7
1090 LPRINT "Slope B7 and its Standard error=";B7 "+-"SB7
1100 LPRINT
1110 LPRINT "Square of maximum correlation coefficient r^2=";MAX
1120 LPRINT "Optimum value of pairs N=";NMAX
1130 LPRINT "Optimum values of points for 1st, 2nd and 3rd exponential

            functions,respectively=";JMAX","GMAX"and"N-JMAX-GMAX
1140 LPRINT "Values of S and P, respectively =";SMAX"and"PMAX
1150 LPRINT
1160 REM Enter DATA in lines 3000-3040 in the order H(peak height), T(min)
3000 DATA
3010 DATA
```

Appendix A. (*Continued*)

```
3020 DATA
3030 DATA
3040 DATA
3050 A1=A5*H1:A2=SMAX*A6*H1:A3=PMAX*A7*H1:B1=B5:B2=B6:B3=B7
3060 A1P=A1*(B1-B2)*(B1-B3)
3070 A2P=A2*(B2-B1)*(B2-B3)
3080 A3P=A3*(B3-B1)*(B3-B2)
3090 A31=A3P/A1P:A21=A2P/A1P
3100 K31=(B3^2-A31*B1^2)/(A31*B1-B3)
3110 K21=(B2^2-A21*B1^2)/(A21*B1-B2)
3120 KAV=(K31+K21)/2
3130 X1=-(B1+B2+B3)
3140 Y1=(B1*B2+B1*B3+B2*B3)
3150 Z1=-(B1*B2*B3)
3160 AA1=2*D1*60/L1^2
3170 Q2=2*L2*AY*E/AZ/L1
3180 INVAA2=1/(X1-KAV)-(1+Q2)/AA1:AA2=1/INVAA2
3190 D2=AA2*L2^2/2
3200 AQ1=AA1+AA2*Q2:AQ2=AA1+AA2+AA2*Q2
3210 K1KR=(Y1*AQ2-AA1*AA2*KAV)/AQ1
3220 K1K2KR=Z1*AQ2/AQ1
3230 K2=K1K2KR/K1KR
3240 KR=KAV-K2
3250 K1=K1KR/KR
3260 LPRINT "Coefficient for Isotherm Integration k1 in 1/s=";K1/60
3270 LPRINT "Adsorption/Desorption Rate Constant kR in 1/s=";KR/60
3280 LPRINT "Surface Reaction Rate Constant k2 in 1/s=";K2/60
3290 LPRINT
3300 LPRINT "Total Diffusion Coefficient in the Solid Bed De(cm^2/s)=";D2/60
3310 LPRINT
3320 A=A1/B1+A2/B2+A3/B3
3330 G1=ABS(V0*A/NB)
3333 MA=K1*AY*E/AS
3336 MD=-D1*G1/LV/L1
3340 LPRINT "Calibration Factor of Detector g'in cm per mol/cm^3=";G1
3350 LPRINT
3360 LPRINT TAB(3);"T";TAB(9);"E1";TAB(20);"DG";TAB(30);"Cs";TAB(39);"Theta";

            TAB(52);"GammaS";TAB(60);"100*PHI(GAMMAS)"
3370 LPRINT TAB(1);"(min)";TAB(7);"(kJ/mol)";TAB(20);"(kJ/mol)";TAB(28);

     "(micromol/g)";TAB(40);"(Dim/less)";TAB(52);"(mJ/m^2)";TAB(62);"(m^2/mJ)
"
3380 LPRINT
3390 Q1=0:Q2=0:Q3=0:Q4=0:Q5=0
3400 FOR T=T1 TO T2 STEP 2
3410 ABT=A1*EXP(B1*T)+A2*EXP(B2*T)+A3*EXP(B3*T)
3420 ABBT=A1*B1*EXP(B1*T)+A2*B2*EXP(B2*T)+A3*B3*EXP(B3*T)
3430 AB2BT=A1*B1^2*EXP(B1*T)+A2*B2^2*EXP(B2*T)+A3*B3^2*EXP(B3*T)
3440 AB3BT=A1*B1^3*EXP(B1*T)+A2*B2^3*EXP(B2*T)+A3*B3^3*EXP(B3*T)
3450 CS=(MA/MD)*(A1*(EXP(B1*T)-1)/B1+A2*(EXP(B2*T)-1)/B2+A3*(EXP(B3*T)-1)/B3)
3460 CY=10^6*ABT/MD
3470 DCY=10^6*ABBT/MD
3480 CC1=(MA/MD)*ABT
3490 CC2=MA*ABT/ABBT/10^6
3500 CC4=MA*(1-ABT*AB2BT/ABBT^2)/10^6
3510 KRT=ABS(MD*(AB2BT/ABBT^2-1/ABT)/10^6)
3520 DKRT=ABS(MD*(ABBT/ABT^2+AB3BT/ABBT^2-2*AB2BT^2/ABBT^3)/10^6)
3530 K=101325!*KRT/8.314/T0
3540 K0=1.218203E-08/T0^2.5/MB^1.5
3550 E1=8.314*T0*LOG(K/K0)
3560 THETA=1-EXP(-KRT*CY)
3570 CSMAX=CS/THETA
3580 DG=-8.314*T0*LOG(K)
3590 NA=2*6.023E+23*CSA*10^-20
3600 GAMMA=-1000*DG/NA
```

Appendix A. (*Continued*)

```
3610 GAMMAS=GAMMA^2/ST
3620 DTHETAT=(KRT*DCY+CY*DKRT)*EXP(-KRT*CY)
3630 DCSMAX=(THETA*CC1-CS*DTHETAT)/THETA^2
3640 DK=101325!*DKRT/8.314/T0
3650 DDG=-8.314*T0*DK/K
3660 FDG=DCSMAX/DDG:PHIDG=ABS(FDG*THETA/CSMAX)
3670 DGAMMA=-1000*DDG/NA
3680 DGAMMAS=2*GAMMA*DGAMMA/ST
3690 FGAMMAS=DCSMAX/DGAMMAS:PHIGAMMAS=ABS(FGAMMAS*THETA/CSMAX)
3700 LPRINT TAB(1);T;TAB(7);E1/1000;TAB(18);DG/1000;TAB(28);CS*10^6;

          TAB(38);THETA;TAB(50);GAMMAS;TAB(62);PHIGAMMAS*100
3710 Q1=Q1+ABS(PHIDG):Q2=Q2+ABS(PHIGAMMAS)
3720 Q3=Q3+ABS(PHIDG)*DG:Q4=Q4+GAMMAS*ABS(PHIGAMMAS)
3730 NEXT T
3740  LPRINT
3750 LPRINT "<DG> in kJ/mol=";Q3/Q1/1000
3760 LPRINT "<GammaS> in mJ/m^2=";Q4/Q2"
3770 END
4000  REM Linear regression of Y(I) = A + B T(I)
4010 S1=0
4020 S2=0
4030 S3=0
4040 S4=0
4050 S5=0
4060    FOR I=K TO L
4070    S1=S1+T(I)
4080    S2=S2+T(I)^2
4090    S3=S3+Y(I)
4100    S4=S4+Y(I)^2
4110    S5=S5+T(I)*Y(I)
4120 NEXT I
4130 Z=L-K+1  :REM Number of points for the linear regression analysis
4140 M1=S5-S1*S3/Z
4150 M2=S2-S1^2/Z
4160 M3=S4-S3^2/Z
4170 A=(S3-S1*M1/M2)/Z
4180 B=M1/M2
4190 SYT=SQR(ABS(S4-A*S3-B*S5)/(Z-2))
4200 SA=SYT*SQR(S2/Z/M2)
4210 SB=SYT/SQR(M2)
4220 RETURN
```

References

[1] D.J. Dwyer, F.M. Hoffmann (Eds.), Surface Science of Catalysis, ACS Symposium Series No. 482, American Chemical Society, Washington, DC, 1992.
[2] N.A. Katsanos, R. Thede, F. Roubani-Kalantzopoulou, J. Chromatogr. A 795 (1998) 133.
[3] D.R. Williams (Guest Editor), J. Chromatogr. A 969 (2002) 1.
[4] N.A. Katsanos, J. Chromatogr. A 969 (2002) 3.
[5] N.A. Katsanos, E. Arvanitopoulou, F. Roubani-Kalantzopoulou, A. Kalantzopoulos, J. Phys. Chem. B 103 (1999) 1152.
[6] J.R. Conder, C.L. Young, Physicochemical Measurement by Gas Chromatography, Wiley, Chichester, 1979, p. 576.
[7] A. Boutboul, F. Lenfant, P. Giampaoli, A. Feigenbaum, V. Ducruet, J. Chromatogr. A 969 (2002) 9.
[8] E. Kalogirou, I. Bassiotis, Th. Artemiadi, S. Margariti, V. Siokos, F. Roubani-Kalantzopoulou, J. Chromatogr. A 969 (2002) 81.
[9] H. Grajek, Z. Witkiewicz, J. Chromatogr. A 969 (2002) 87.
[10] G.M. Dorris, D.G. Gray, J. Colloid. Interf. Sci. 77 (1980) 353.
[11] M. Nardin, E. Papirer, J. Colloid. Interf. Sci. 137 (1990) 534.
[12] T. Hamieh, M. Rezzaki, J. Schultz, Colloid Surf. A 189 (2001) 279.
[13] D.J. Williams (Guest Editor), J. Chromatogr. A 969 (2002) 17, 59, 215.
[14] W. Rudzinski, D.H. Everett, Adsorption of Gases on Heterogeneous Surfaces, Academic Press, London, 1992.
[15] N.A. Katsanos, F. Roubani-Kalantzopoulou, Adv. Chromatogr. 40 (2000) 231.
[16] N.A. Katsanos, Flow Perturbation Gas Chromatography, Marcel Dekker, New York, 1988.
[17] J. Roles, G. Guiochon, J. Chromatogr. 591 (1992) 233.
[18] B. Stanley, G. Guiochon, J. Phys. Chem. 97 (1993) 8098.
[19] S. Golshan-Shirazi, G. Guiochon, J. Chromatogr. A 670 (1994) 1.
[20] B.J. Stanley, G. Guiochon, Langmuir 10 (1994) 4278;
B.J. Stanley, G. Guiochon, Langmuir 11 (1995) 1735.
[21] I. Quinones, G. Guiochon, J. Colloid Interf. Sci. 183 (1996) 57.
[22] M. Heuchel, M. Jaroniec, R.K. Gilpin, J. Chromatogr. 628 (1993) 59.
[23] M. Jaroniec, R. Madey, Physical Adsorption on Heterogeneous Solids, Elsevier, Amsterdam, 1988.
[24] N.A. Katsanos, E. Iliopoulou, V. Plagianakos, H. Mangou, J. Colloid Interf. Sci. 239 (2001) 10.
[25] A.W. Adamson, A.P. Gast, Physical Chemistry of Surfaces, 6th edition, Wiley, New York, 1997, p. 655.
[26] A.W. Adamson, Colloids Surf. A 118 (1996) 193.
[27] A.W. Adamson, I. Ling, Adv. Chem. 33 (1961) 51.
[28] W.A. House, M.J. Jaycock, Colloid Polym. Sci. 256 (1978) 52.
[29] J. Jagiello, Langmuir 10 (1994) 2778.

[30] N.A. Katsanos, E. Iliopoulou, F. Roubani-Kalantzopoulou, E. Kalogirou, J. Phys. Chem. B 103 (1999) 10228.
[31] N.A. Katsanos, N. Rakintzis, F. Roubani-Kalantzopoulou, E. Arvanitopoulou, A. Kalantzopoulos, J. Chromatogr. A 845 (1999) 103.
[32] F. Roubani-Kalantzopoulou, Th. Artemiadi, I. Bassiotis, N.A. Katsanos, V. Plagianakos, Chromatographia 53 (2001) 315.
[33] D.S. Jovanovic, Colloid Polym. Sci. 235 (1969) 1203, 1214.
[34] Ch. Abatzoglou, E. Iliopoulou, N.A. Katsanos, F. Roubani-Kalantzopoulou, A. Kalantzopoulos, J. Chromatogr. A 775 (1997) 211.
[35] N.A. Katsanos, D. Gavril, G. Karaiskakis, J. Chromatogr. A 983 (2003) 177.
[36] N. Bakaoukas, A. Koliadima, L. Farmakis, G. Karaiskakis, N.A. Katsanos, Chromatographia 57 (2003) 783.
[37] S. Margariti, N.A. Katsanos, F. Roubani-Kalantzopoulou, Colloid Surf. A 226 (2003) 55.
[38] N.A. Katsanos, D. Gavril, J. Kapolos, G. Karaiskakis, J. Colloid Interf. Sci., in press.
[39] V. Sotiropoulou, G.P. Vassilev, N.A. Katsanos, H. Metaxa, F. Roubani-Kalantzopoulou, J. Chem. Soc., Faraday Trans. 91 (1995) 485.
[40] R.P. Bird, W.E. Stewart, E.N. Lightfoot, Transport Phenomena, Wiley, Chichester, 1960, p. 511.
[41] N.A. Katsanos, F. Roubani-Kalantzopoulou, E. Iliopoulou, I. Bassiotis, V. Siokos, M.N. Vrahatis, V.P. Plagianakos, Colloids Surf. A 201 (2002) 173.
[42] J.D. Hazlett, C.C. Hsce, B.W. Wojcienchowski, J. Chem. Soc. Faraday Trans. 275 (1979) 602.
[43] W. Rudzinski, B.W. Wojciechowski, J. Colloid Polym. Sci. 255 (1977) 869, 1086.
[44] S. Sircar, J. Colloid Interf. Sci. 101 (1984) 452.
[45] M. Jaroniec, S. Sokolowski, A. Waksmundzki, Pol. J. Chem. 50 (1976) 779.
[46] U. Landman, E.W. Montroll, J. Chem. Phys. 64 (1976) 1762.
[47] S.J. Gregg, K.S.W. Sing, Adsorption Surface Area and Porosity, Academic Press, London, 1967, p. 67.
[48] Y.A. Bakaev, W.A. Steele, Langmuir 8 (1992) 1372.
[49] N.A. Katsanos, F. Roubani-Kalantzopoulou, Annales Universitatis Mariae Curie-Sklodowska, Chemia LVII (2002) 101.
[50] E. Vicke, R. Kallenbanh, Kolloid-Z. 17 (1941) 135.
[51] A. Kapoor, R.T. Yang, C. Wong, Catal. Rev.-Sci. Eng. 31 (1989) 129.
[52] J.M. Smith, in: Chemical Engineering Kinetics, 3rd edition, McGraw-Hill, New York, 1981, p. 471.
[53] K. Higashi, H. Ito, J. Oishi, J. Nucl. Sci. Tech. 1 (1964) 293.
[54] D. Gavril, G. Karaiskakis, J. Chromatogr. A 845 (1999) 67.
[55] D. Gavril, N.A. Katsanos, G. Karaiskakis, J. Chromatogr. A 852 (1999) 507.
[56] D. Gavril, A. Koliadima, G. Karaiskakis, Chromatographia 49 (1999) 585.
[57] D. Gavril, A. Koliadima, G. Karaiskakis, Langmuir 15 (1999) 3798.
[58] D. Gavril, J. Liq. Chromatogr. R. T. 25 (2002) 2079.
[59] D. Gavril, Instrum. Sci. Technol. 30 (2002) 397.
[60] V. Loukopoulos, D. Gavril, G. Karaiskakis, Instrum. Sci. Technol. 31 (2003) 165.
[61] A. Voelkel, in: A. Dabrowski, V.A. Tertykh (Eds.), Adsorption on New and Modified Inorganic Sorbens. Studies in Surface Science and Catalysis, vol. 99, Elsevier, Amsterdam, 1996, p. 465.
[62] G.M. Dorris, D.G. Gray, J. Colloid Interf. Sci. 71 (1979) 931.
[63] F.M. Fowkes, J. Colloid Interf. Sci. 28 (1968) 493.
[64] V.I. Bogillo, A. Voelkel, J. Adhes. Sci. Technol. 11 (1997) 1513.
[65] V.I. Bogillo, V.V. Turov, A. Voelkel, J. Adhes. Sci. Technol. 11 (1997) 1531.
[66] V.I. Bogillo, V.P. Shkilev, A. Voelkel, J. Mater. Chem. 8 (1998) 1953.
[67] D.R. Williams (Guest Editor), J. Chromatogr. A 969 (2002) 17, 27, 49, 59, 215.
[68] A.R. Bishop, G.S. Girola, R.G. Nuzzo, J. Phys. Chem. B 104 (2000) 747.
[69] R.H. Perry, C.H. Hilton, Chemical Engineers Handbook, McGraw-Hill, Kogakusha, 1973, pp. 3–240.